

Chapter 9 -- Configuration Flexibility and Robustness

9.1 Introduction

In order to achieve the scientific goals of the NCSX mission, the NCSX device must be capable of supporting a range of variations in plasma configuration about the reference baseline equilibrium. In the following sections we demonstrate the robustness and flexibility of NCSX.

As described in Chapter 2 the NCSX coil system was designed in a two-stage approach. In the first stage, a reference physics configuration was identified with attractive physics properties (the S3 state of li383). In the second stage, coils were reverse-engineered in such a way that the physics properties of the reference configuration were reproduced as accurately as possible, consistent with engineering constraints, in a free-boundary reconstruction of the plasma.

Figure 9-1 shows a top view of the modular coil set M1017 used for the flexibility and robustness studies presented here. There are 7 coils in each of the three periods of the machine. Stellarator symmetry implies that within any given period only 4 coil currents are independent. The independent coils are labeled “1”, “2”, “3” and “4”. Stellarator-symmetric partners are labeled with prime superscripts. The same numbering convention will be used to identify the coils when presenting coil current solutions in our flexibility studies.

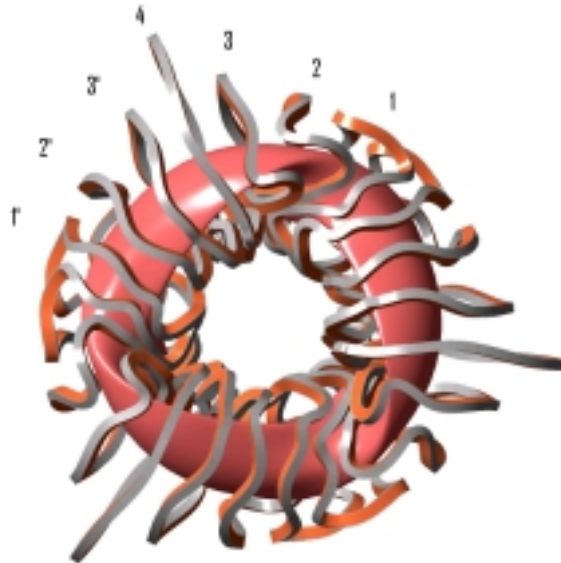


Figure 9-1: Modular coilset M1017 used for flexibility and robustness studies. Integers “1”, “2”, “3” and “4” label the four coils within each period whose coil currents are allowed to vary independently of one another. Coil k' is the mirror symmetric partner of coil k

NCSX plans to allow the four modular coil currents to vary independently; thus the mean (toroidally averaged) toroidal magnetic field at a given radius will also vary. For systematic experiments it is advantageous to separate the provision of external transform by 3D shaping from provision by changes in the average toroidal field. In principle, the average toroidal field can be constrained to be a constant value by varying only three linear combinations of the four modular coil currents. However we have found that this leads to a considerable reduction in the flexibility of NCSX to control the external transform. For this reason NCSX plans to include an auxiliary TF coil system where the TF coil current is allowed to vary together with the four modular coil currents in such a way that the mean TF field remains constant.

In the flexibility calculations presented in this Chapter, the auxiliary toroidal field coil is modeled as a single vertical wire filament on the machine centerline ($R=0$). A filament current of $I_T = 7.0 \times 10^6$ Amps produces an auxiliary TF field of $B_T = 1.0$ T at the radius $R = 1.4$ m.

In addition to the five independent coil systems mentioned so far, a system of axisymmetric poloidal field currents is included for additional flexibility. For the flexibility studies presented here, the poloidal fields are included as a superposition of the lowest four axisymmetric multipoles (Dipole, Quadrupole, Hexapole and Octapole). Candidate poloidal field coilsets are evaluated by fitting to the multipole fields output by the free-boundary optimizer. Once the range of multipole fields required to produce configurations which span the desired operating space is known, a discrete poloidal field coil system will be designed where the coils are placed in optimal locations subject to the known accessibility constraints for diagnostics and beam access, etc. The expansion point for the multipole fields is $R = 1.4$ m, $Z = 0.0$ m, and units for these fields are such that $\mu_0 B_0 = 1$.

The reference li383 S3 plasma configuration ($I_p = 174$ kA, $B_T = 1.7$ T at $R = 1.4$ m) assumes bootstrap consistency between the current and pressure profiles. These 'reference' profiles are shown in Figure 9-2. The reference configuration shape was derived using a fixed-boundary optimizer. For fixed values of β , I_p and B_T , the optimizer adjusts the shape of the plasma boundary to minimize a physics objective function which includes measures of quasi-axisymmetry, and of kink, ballooning, and Mercier mode stability - see Chapter 2. For li383, the β -limit is 4.2%.

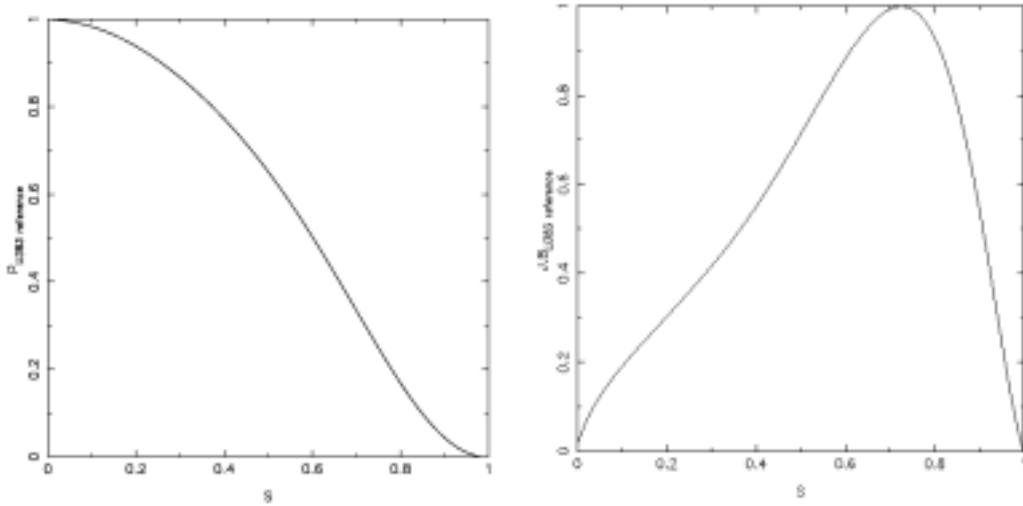


Figure 9-2: Baseline ‘reference’ current (J.B) and pressure (p) profiles as a function of normalized toroidal flux, s

The VMEC based free-boundary optimizer is used to determine coil currents which produce a free-boundary equilibrium consistent with a chosen set of plasma profiles. The cost function minimized by the optimizer is a weighted sum of $\chi^2_{Bmn} = \sum' B_{mn}^2/B_{00}^2$, a measure of the degree of quasi-axisymmetry of the plasma (the B_{mn} are Fourier components of the magnetic field analysed on the $s=0.25$, $s=0.50$, and $s=0.75$ magnetic surfaces evaluated in Boozer magnetic coordinates; the summation is over modes with $n>0$), $\chi^2_K = \lambda_K^2$ (the square of the unstable eigenvalue of the dominant kink instability evaluated by the TERPSICHORE stability code), and $\chi^2_B = \sum \lambda_B^2$ (the sum of squares of the maximum ballooning eigenvalue on any of the 49 magnetic surfaces used in the calculation of VMEC equilibria). Optimized equilibria are constrained to be tangent at some point to a three-dimensional first wall boundary whose normal separation distance from the plasma to the reference li383 plasma configuration is defined (as a function of poloidal angle u) by

$$\begin{aligned} \rho_{sep}(u) &= 10.0 - 20.0*u \text{ cm} & \text{for} & \quad 0.0 < u < 0.4, \\ &= 2.0 \text{ cm} & \text{for} & \quad 0.4 < u < 1.0 \end{aligned}$$

for all toroidal angles v . This limiter surface is a surrogate for the eventual plasma facing component boundary.

The reference profiles of current and pressure define a single point in the operating space of NCSX. In the following subsections we address the following questions on robustness and performance:

- How does the plasma performance change as profiles are changed from the reference?
- Is the operating space for configurations with adequate performance characteristics wide enough to allow fulfillment of the NCSX mission?
- Can the designed coils produce the magnetic fields required to support this range of plasma configurations?

9.2 Robustness of Plasma Shape and Position

Execution of planned experiments will require pre-programming of coil current (or voltage) waveforms. Accurate prediction of plasma profiles is unlikely during initial experimental campaigns, therefore pre-programmed coil currents will only be approximately consistent with actual profiles. Plasma shape and position will likely differ from expectation.

It is appropriate to ask whether equilibria obtained using estimated coil currents will have positions and shapes that are sufficiently close to the desired configuration that recovery by feedback control is possible. To address this question free-boundary equilibria were calculated for a variety of pressure and current profile shapes, net plasma toroidal current and plasma beta, using coil currents set equal to values appropriate to the reference S3 state of li383.

Three pressure profiles denoted by $p_A(s)$, $p_B(s)$, $p_C(s)$ expressed as a function of the normalized toroidal flux s were selected from a collection of measured profiles obtained on four stellarators (ATF, CHS, LHD, W7-AS) and two tokamaks (PBX-M, DIII-D) which bracket NCSX in size[1]. The selected profiles cover the plausible range of pressure peakedness/broadness that can be expected to occur in NCSX. The peaked profile, $p_A(s)$, is taken from an NBI heated L-mode discharge on DIII-D (shot 78109); the broad profile, $p_C(s)$, is taken from an NBI heated CHS discharge (shot C_MC2). It is similar to the assumed baseline li383 profile used for the NCSX design studies. The intermediate profile, $p_B(s)$ corresponds to an NBI heated discharge on PBX-M (shot 3113_1). Plots of the selected $p_j(s)$ are shown in Figure 9-3.

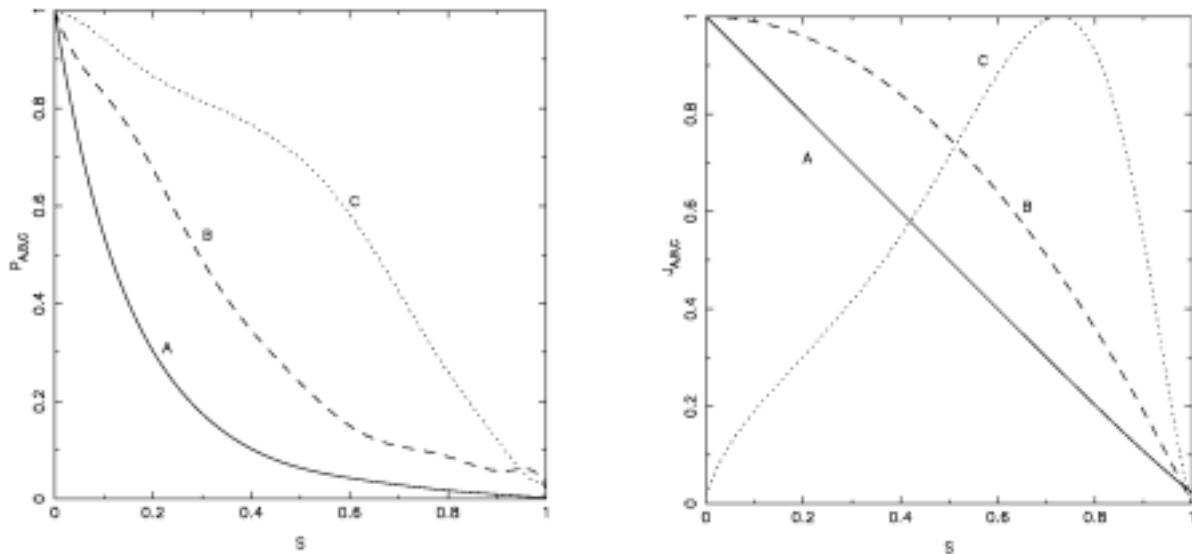


Figure 9-3: Three profiles of pressure ($p_A(s)$, $p_B(s)$, $p_C(s)$) and three profiles of parallel current by ($J_A(s)$, $J_B(s)$, $J_C(s)$) used for shape robustness calculations

Three profiles of parallel current $\mathbf{J} \cdot \mathbf{B}(s)$ denoted by $J_A(s)$, $J_B(s)$, $J_C(s)$ were also selected which cover a wide range of current peakedness/broadness. They are also shown in Figure 9-3. The peaked and intermediate current profiles have the analytic forms $J_A(s) = 1 - s$ and $J_B(s) = 1 - s^2$, respectively. The broad current profile, $J_C(s)$, is identical to the hollow li383 reference current profile.

Free-boundary equilibria were calculated for the nine possible combinations of plasma current and pressure profiles corresponding $I_p = 174$ kA, $B_T = 1.7$ T and a beta value of $\beta = 4.2\%$ using the coil currents shown in Table 9-1. Plasma boundaries for the nine reconstructions are shown in Figure 9-4, as are the calculated profiles of rotational transform, $\iota(s)$.

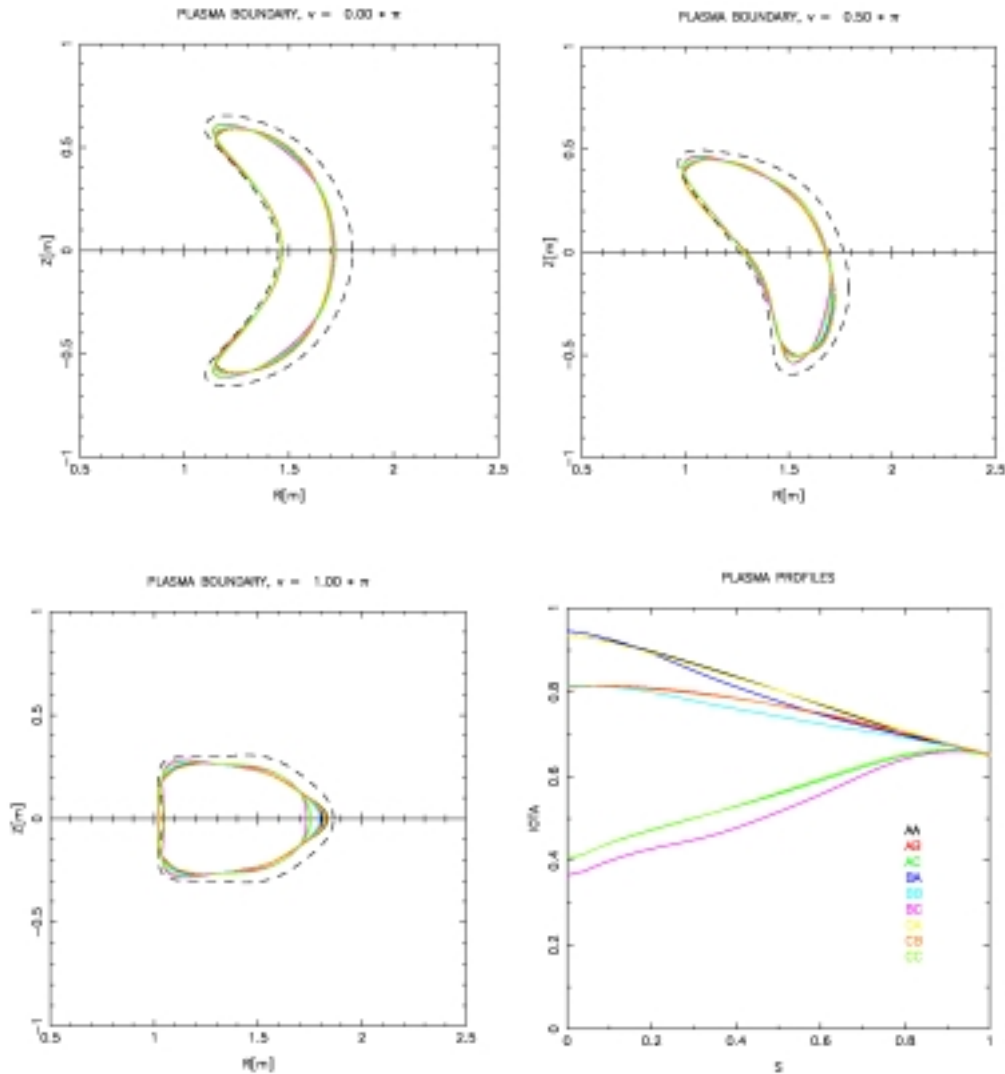


Figure 9-4: Reconstructed plasma boundaries for nine combinations of pressure and current profile with $I_p = 174$ kA, $B_T = 1.7$ T, $\beta = 4.2\%$, using fixed S3 ($\beta=4.2\%$) coil currents. Boundaries are shown at three toroidal cross sections. The dashed curve represents the first wall boundary; it is not used as a limiter constraint in the calculations. Profiles of rotational transform are also shown

The three groups of iota profiles correspond to the three current profiles. Members of each group differ primarily in their axis value, $\iota(0)$. Variations within each group are due to the variations in pressure profile. The first-wall boundary is shown as a dashed curve to indicate the scale of variation of the boundary shapes. However this first wall boundary was not treated as a limiter surface for the calculated equilibria. The variation in plasma shape and position for this wide range of equilibrium profiles is seen to be modest.

AUX TF [A]	MOD 1 [A]	MOD 2 [A]	MOD 3 [A]	MOD 4 [A]	PF - DIPOLE	PF - QUAD	PF - HEX	PF - OCT
0	-5.670e+5	-5.670e+5	-5.670e+5	-5.670e+5	0	0	0	0

Table 9-1: Coil currents used for shape/position robustness calculations. The auxiliary TF and PF coil currents are zero, and the modular coil currents are equal. The modular coil currents were provided by the engineering coil design code COILOPT

	$\mathbf{J_A}$	$\mathbf{J_B}$	$\mathbf{J_C}$
$\mathbf{P_A}$	$\chi^2_{\text{BMN}} = 0.032$ $\epsilon_h [\%] = 1.46, 5.07, 9.70$	$\chi^2_{\text{BMN}} = 0.024$ $\epsilon_h [\%] = 0.71, 2.88, 6.43$	$\chi^2_{\text{BMN}} = 0.020$ $\epsilon_h [\%] = 0.27, 0.64, 1.44$
$\mathbf{P_B}$	$\chi^2_{\text{BMN}} = 0.036$ $\epsilon_h [\%] = 3.10, 5.64, 7.54$	$\chi^2_{\text{BMN}} = 0.025$ $\epsilon_h [\%] = 1.74, 3.63, 5.49$	$\chi^2_{\text{BMN}} = 0.023$ $\epsilon_h [\%] = 0.33, 0.62, 1.22$
$\mathbf{P_C}$	$\chi^2_{\text{BMN}} = 0.028$ $\epsilon_h [\%] = 0.93, 3.56, 7.97$	$\chi^2_{\text{BMN}} = 0.022$ $\epsilon_h [\%] = 0.58, 2.32, 5.74$	$\chi^2_{\text{BMN}} = 0.020$ $\epsilon_h [\%] = 0.26, 0.59, 1.37$

Table 9-2: Measures of quasi-axisymmetry for un-optimized free-boundary equilibria with various combinations of pressure and current profile, using fixed coil currents. $\chi^2_{\text{Bmn}} = \Sigma' B^2_{\text{mn}}/B^2_{00}$ is the QA-measure used in the optimizer; ϵ_h is the effective helical ripple strength evaluated at normalized toroidal flux values of $s = 0.25, 0.50,$ and 0.75

Table 9-2 presents calculated values of the quasi-axisymmetry measure $\chi^2_{\text{Bmn}} = \Sigma' B^2_{\text{mn}}/B^2_{00}$ for the un-optimized equilibria shown in Figure 9-4 (the equilibria are “un-optimized” in the sense that no attempt is made to improve the quality of the plasma parameters by allowing coil currents to vary). Also presented are values of ϵ_h , the effective helical ripple strength (see Chapter 8) evaluated at the three values of normalized toroidal flux $s = 0.25, 0.50,$ and 0.75 . These values of s correspond to values of normalized radius r/a of approximately $0.50, 0.70,$ and 0.85 , respectively. The χ^2_{Bmn} values can be compared with the value 0.015 obtained for the li383 S3 reference configuration (Chapter 3, section 3.2.5) and the ϵ_h values can similarly be compared with the values $0.15\%, 0.61\%,$ and 1.73% for the reference fixed boundary configuration. A large degradation in quasi-axisymmetry occurs when the current profile becomes more peaked.

A mild degradation in QA-ness occurs as the pressure profile is peaked. A correlation between χ^2_{Bmn} and ϵ_h is seen, but it is less than perfect. For example, the degradation in χ^2_{Bmn} between the profile combination p_B, J_C and p_B, J_B is mild, yet the degradation in values of ϵ_h is substantial. In subsequent sections of this Chapter, we will therefore quote values of the calculated effective ripple amplitude, and omit quotation of χ^2_{Bmn} .

Figure 9-5 compares plasma boundaries for reconstructed plasmas using reference profiles but different values of β and I_p . Coil currents are again fixed at li383 reference S3 values. The boundary shown in black corresponds to an S3 state with $I_p = 174$ kA, $\beta = 4.2\%$. The other two boundaries correspond to imagined disruptions where the plasma is assumed to have instantaneously lost all of its β or all of its current: The plasma boundary shown in red corresponds to the case of a post β -collapse $I_p = 174$ kA, $\beta = 0.0\%$, while the boundary shown in green corresponds to the even more extreme limit where all the plasma current is lost; $I_p = 0$ kA, $\beta = 4.2\%$. The position/shape changes seen in Figure 9-5 can be contrasted with the behavior of tokamaks under equivalent changes of I_p and/or β where the loss of positional equilibrium would be much more severe. In the actual NCSX experiment, radial loss of equilibrium will be opposed by provision of an increased vertical (e.g., dipole) field.

Case	QA-ness measures
$I_p = 174$ kA, $\beta = 4.2\%$	$\chi^2_{\text{BMN}} = 0.020$ $\epsilon_h [\%] = 0.27, 0.67, 1.57$
$I_p = 174$ kA, $\beta = 0.0\%$	$\chi^2_{\text{BMN}} = 0.068$ $\epsilon_h [\%] = 0.33, 0.59, 2.12$
$I_p = 0$ kA, $\beta = 4.2\%$	$\chi^2_{\text{BMN}} = 0.043$ $\epsilon_h [\%] = 0.34, 1.24, 2.95$

Table 9-3: Quasi-axisymmetry measures χ^2_{Bmn} and ϵ_h for equilibria with various plasma current and beta values

It should be noted that each of the un-optimized equilibria corresponding to the data in Table 9-2 is unstable to kink modes at the given values of β . Even when we add to each equilibrium a sufficient dipole field to maintain radial position, the equilibria are found to be unstable. In NCSX, as in tokamaks, we must expect to change the plasma shape in response to changes in coil currents if we are to maintain stability as β , plasma current, I_p , or profile shapes (e.g., internal inductance ℓ_i) are changed.

In the following Sections, we investigate the performance of plasmas whose profiles and/or beta and net toroidal current differ from their reference forms and/or values. Coil currents are allowed to vary in such a way that χ^2_{Bmn} is minimized while kink and ballooning stability are enforced and plasmas are constrained to be limited by the first wall boundary. We will show that in spite of these constraints, stable plasmas with good quasi-axisymmetry can be obtained for a wide range of assumed plasma conditions.

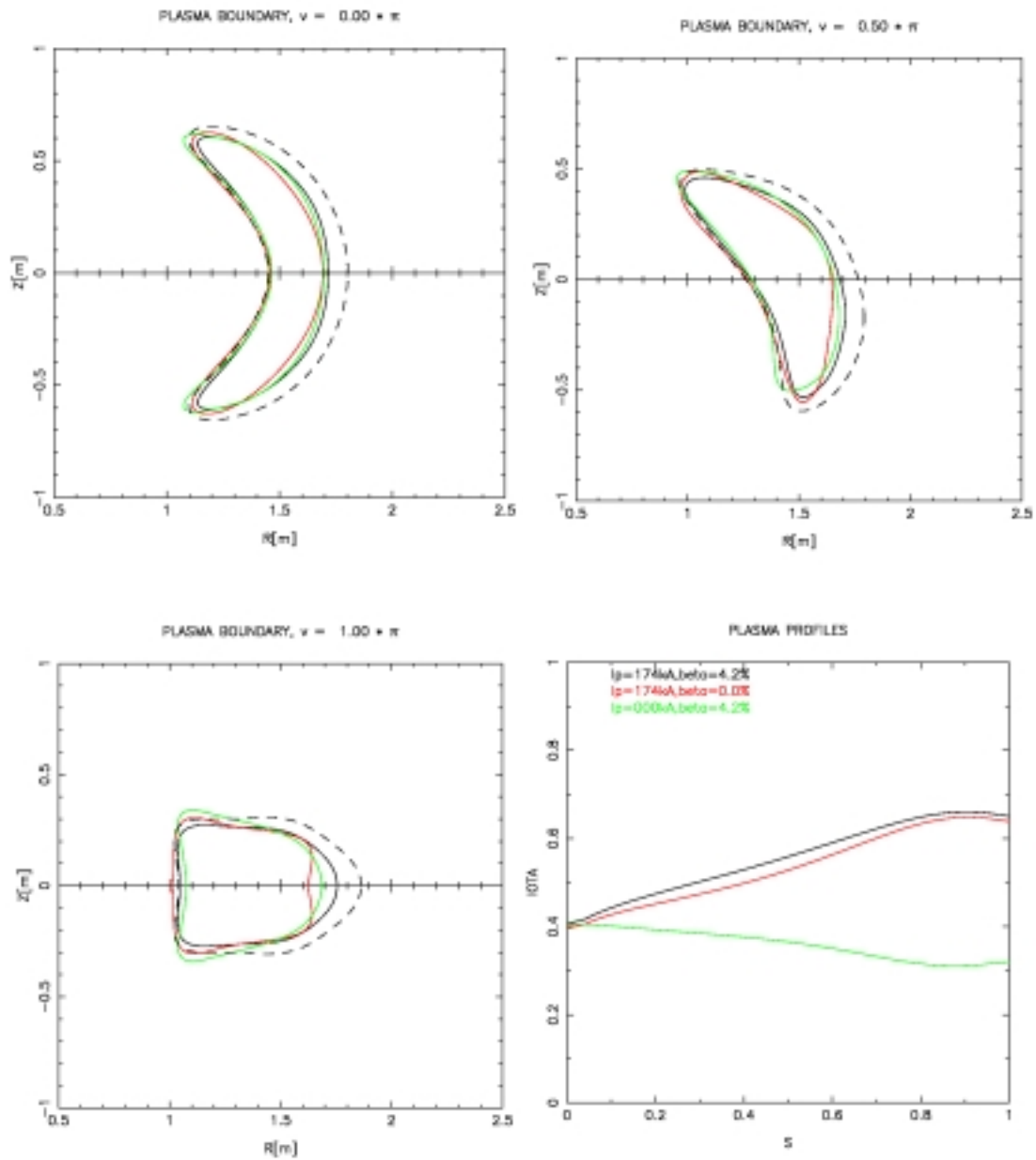


Figure 9-5: Overlay of plasma boundaries for reconstructed equilibria with reference profiles and various I_p , β values: $(I_p, \beta) = (174 \text{ kA}, 4.2\%), (174 \text{ kA}, 0.0\%),$ and $(0 \text{ kA}, 4.2\%)$. As in Figure 9-4, no limiter constraint was imposed

9.3 Robustness of Performance as β and I_p are Varied

In Chapter 10, discharge simulations are presented as a sequence of free-boundary equilibria corresponding to the “evolution” of an NCSX plasma from a particular S1 state where $\beta = 0.0\%$ to a final S3 state where $\beta = 4.2\%$. Pressure profile evolution is consistent with a 1-D transport model. The evolution from initial to final states can be represented as a curve on an $I_p - \beta$ plane. Each point on the curve is associated with a particular profile of plasma current and pressure.

In this section, we explore the robustness of performance of NCSX plasmas produced with M1017 coils. The free-boundary optimizer is run for a range of values of β and I_p using reference S3 profiles of current and pressure (Figure 9-2). In each case coil currents were varied to produce shape deformations of the plasma that lead to the minimization of a linear combination of χ^2_{Bmn} and the (square of the) growth rates for kink and ballooning modes. The average toroidal field was constrained to be constant, with $B_T = 1.7$ T at $R=1.4$ m.

Results are presented in Table 9-4. In each block is listed the kink and ballooning mode stability characteristics of the optimized configuration, as well as the effective helical ripple strength, $\epsilon_h[\%]$, evaluated on the $s=0.25$, $s=0.5$, and $s=0.75$ magnetic surfaces. Stable free-boundary equilibria were found for nearly every case in the calculated $I_p - \beta$ plane. All equilibria were stable to ballooning modes; nearly all equilibria were stable to kink modes. For $I_p = 174$ kA the free-boundary equilibrium with $\beta = 5.0\%$ was stable to both ballooning and kink modes. This β value is substantially higher than the reference li383 fixed boundary β -limit. We have not yet made a full exploration of the maximum β -limit using the M1017 coils. However, for a related modular coilset, named M0907, stable free-boundary equilibria were found through $\beta = 6.5\%$ (without allowing for the luxury of optimizing profiles). In four cases the kink modes were not completely stabilized by the optimizer. These appear in the yellow blocks of Table 9-4 and correspond to $I_p = 130.5$ kA, $\beta = 2.0\%$, $I_p = 130.5$ kA, $\beta = 2.0\%$, $I_p = 174$ kA, $\beta = 1.0\%$, and $I_p = 174$ kA, $\beta = 2.0\%$. It is likely that by adjusting the relative weights of χ^2_{Bmn} and χ^2_{K} in the physics objective function used by the optimizer the four slightly unstable equilibria of Table 9-4 can be stabilized at some modest cost to the QA-ness. With regard to the QA-ness, ϵ_h values displayed in Table 9-4 were never greater than 2.1% for the $s=0.5$ surface. Typical values are less than 1.5%. As discussed in Chapter 8, it is expected that for this magnitude of ripple amplitude, and with standard conditions of plasma temperature and density, the helical ripple transport will be small compared with axisymmetric neoclassical transport

Using reference profiles, we conclude there is a substantial region of stability with good QA-ness in the $I_p - \beta$ plane.

An overlay of the plasma boundaries and calculated iota profiles for the optimized equilibria obtained in the $I_p - \beta$ scan are presented in Figure 9-6. The range of variation for the coil currents which produce the optimized configurations of the $I_p - \beta$ scan are presented in Table 9-5. For the modular coil currents this variation is less than 15% of the nominal S3 currents (Table 9-1).

β [%]	0.0	1.0	2.0	3.0	4.0	5.0
I_p [kA]						
0						
43.5		$\lambda_{0,1}^K = S$ $\lambda^B = S$ ϵ_h [%] = 0.64 2.11 5.39	$\lambda_{0,1}^K = S$ $\lambda^B = S$ ϵ_h [%] = 0.36 1.30 3.21	$\lambda_{0,1}^K = S$ $\lambda^B = S$ ϵ_h [%] = 0.44 1.30 2.90	$\lambda_{0,1}^K = S$ $\lambda^B = S$ ϵ_h [%] = 0.23 0.86 2.17	
87		$\lambda_{0,1}^K = S$ $\lambda^B = S$ ϵ_h [%] = 0.36 1.56 4.26	$\lambda_{0,1}^K = S$ $\lambda^B = S$ ϵ_h [%] = 0.38 1.60 4.08	$\lambda_{0,1}^K = S$ $\lambda^B = S$ ϵ_h [%] = 0.41 1.28 3.04	$\lambda_{0,1}^K = S$ $\lambda^B = S$ ϵ_h [%] = 0.23 0.86 2.18	
130.5		$\lambda_{0,1}^K = S$ $\lambda^B = S$ ϵ_h [%] = 0.21 0.77 2.11	$\lambda_{0,1}^K = S$ $\lambda_{0,1}^B = -6.0e-5$ $\lambda_{0,1}^K = -2.7e-5$ $\lambda^B = S$ ϵ_h [%] = 0.23 0.84 2.21	$\lambda_{0,1}^K = S$ $\lambda_{0,1}^B = -8.8e-6$ $\lambda_{0,1}^K = -2.2e-5$ $\lambda^B = S$ ϵ_h [%] = 0.50 1.14 2.66	$\lambda_{0,1}^K = S$ $\lambda^B = S$ ϵ_h [%] = 0.20 0.67 1.49	
174	$\lambda_{0,1}^K = S$ $\lambda^B = S$ ϵ_h [%] = 0.33 0.79 2.45	$\lambda_{0,1}^K = S$ $\lambda_{0,1}^B = -1.9e-5$ $\lambda_{0,1}^K = -2.0e-5$ $\lambda^B = S$ ϵ_h [%] = 0.34 0.81 1.97	$\lambda_{0,1}^K = S$ $\lambda_{0,1}^B = -2.3e-5$ $\lambda_{0,1}^K = -2.3e-5$ $\lambda^B = S$ ϵ_h [%] = 0.44 1.43 3.32	$\lambda_{0,1}^K = S$ $\lambda^B = S$ ϵ_h [%] = 0.23 0.79 2.03	$\lambda_{0,1}^K = S$ $\lambda^B = S$ ϵ_h [%] = 0.39 1.29 3.18	$\lambda_{0,1}^K = S$ $\lambda^B = S$ ϵ_h [%] = 0.93 1.66 3.50

Table 9-4: NCSX plasma performance for various β , I_p values. The kink eigenvalues for the $n=0$ and $n=1$ family of kink modes are denoted by $\lambda_{0,1}^K$, $\lambda_{0,1}^B$, respectively, and are tabulated if the mode is found to be unstable. In the case of kink stability, the notation $\lambda_{0,1}^K = S$ is used. $\lambda^B = S \Rightarrow$ no unstable ballooning modes were found. Yellow blocks denote configurations which are found to be unstable to either kink or ballooning modes. The effective helical ripple strength, ϵ_h , is calculated for the $s=0.25$, $s=0.5$, and $s=0.75$ magnetic surfaces

It is interesting to contrast the free-boundary optimization results shown in Table 9-4 with corresponding fixed-boundary results shown in Table 9-6. Here, the stability of plasmas with different I_p , β values is calculated in the fixed li383 S3-state stellarator boundary. The plasma boundary shape is not allowed to change as β and I_p vary. We see that for the fixed-boundary runs there are many more unstable cases than in the free-boundary runs, and choosing a stable path from low β , low I_p to a final state defined as $\beta = 4.0\%$, $I_p = 174$ kA is problematic. The freedom allowed in the free-boundary runs of adjusting the 3D shape to accommodate MHD stability is clearly significant and will be explored in subsequent sections.

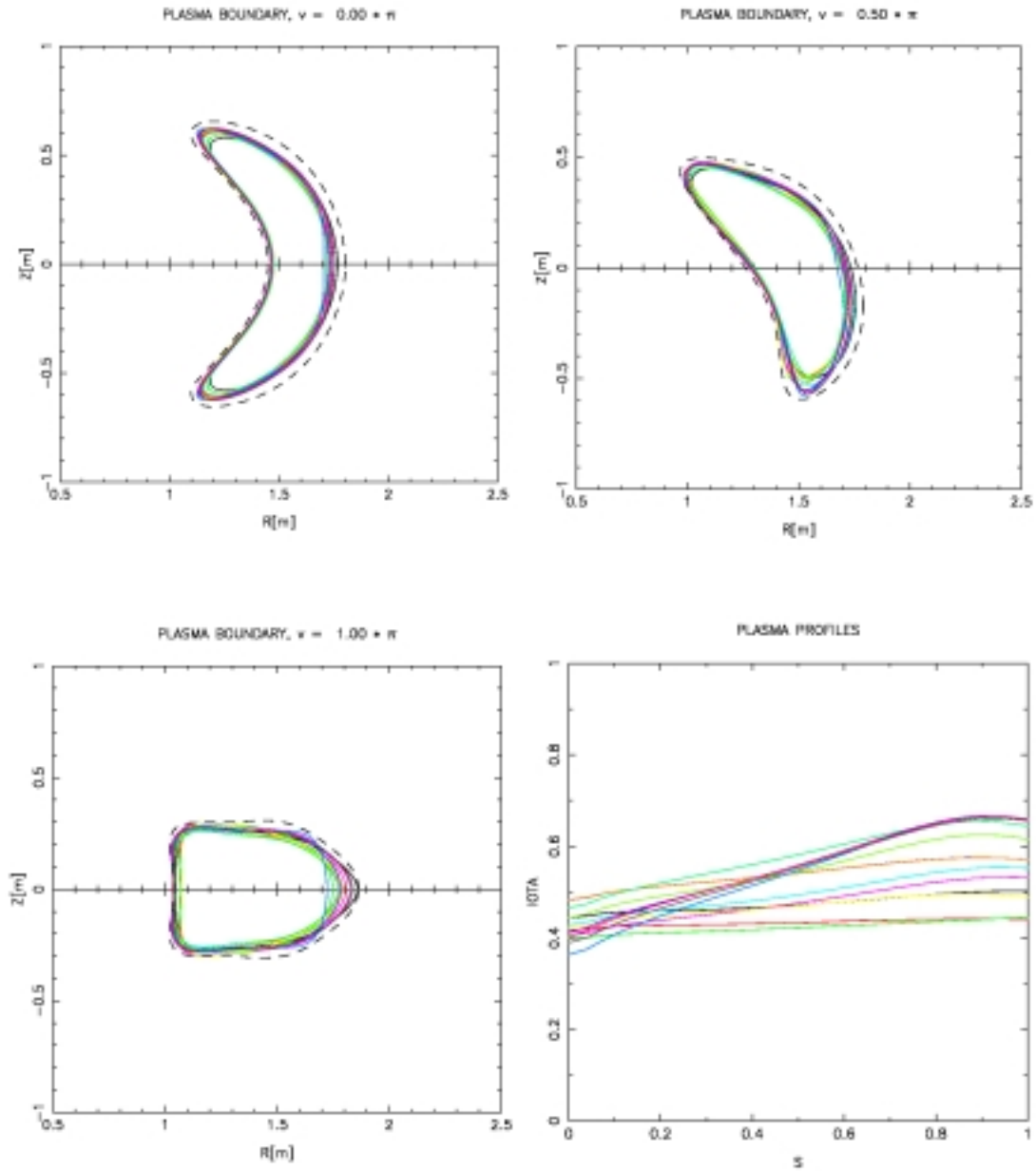


Figure 9-6: Overlay of plasma boundaries, and calculated iota profiles for stable optimized equilibria obtained of the optimized free-boundary $I_p - \beta$ scan. Note the wide range of iota profiles (shear and edge iota values) for which plasmas were found to be stable

	MIN. I _C [A]	CASE	MAX. I _C [A]	CASE
Aux TF [A]	-7.172e+5	i0870b40	+7.088e+3	i1305b40
Mod 1 [A]	-6.110e+5	i0435b40	- 5.577e+5	i1305b40
Mod 2 [A]	-6.311e+5	i0435b40	- 5.566e+5	i0870b20
Mod 3 [A]	-6.157e+5	i0870b40	- 5.268e+5	i0435b10
Mod 4 [A]	-6.350e+5	i0435b10	- 4.811e+5	i1305b30
PF Dipole	+6.478e-2	i0435b40	+ 5.868e-1	i0435b10
PF Quad	- 1.234e-1	i0435b30	+ 9.444e-1	i1305b30
PF Hex	- 6.159e-1	i0435b10	+ 2.142e-0	i0870b30
PF Oct	- 7.319e-0	i1740b10	+ 1.564e-0	i0435b30

Table 9-5: Maximum and Minimum coil currents for the set of optimized configurations in the I_p – β scan experiments. For each case an identifier of the form "ixby" is given, where x/10 is the value of the current in kA, and y/10 is the value of plasma beta in %

β[%] I _p [KA]	0.0	1.0	2.0	3.0	4.0	5.0
0.0	λ ^K _{0,1} = S λ ^B = S					
43.5	λ ^K _{0,1} = S λ ^B = S	λ ^K _{0,1} = S λ ^B = S	λ ^K _{0,1} = S λ ^B = S	λ ^K ₀ = S λ ^K ₁ = -3.5e-4 λ ^B = U ₁₃₋₁₆	λ ^K ₀ = S λ ^K ₁ = -1.5e-3 λ ^B = U ₉₋₁₈	
87	λ ^K ₀ = S λ ^K ₁ = -1.4e-4 λ ^B = S	λ ^K _{0,1} = S λ ^B = S	λ ^K _{0,1} = S λ ^B = S	λ ^K _{0,1} = S λ ^B = S	λ ⁰ _k = S λ ¹ _k = -7.8e-4 λ ^B = U ₄₆₋₄₇	
130.5	λ ^K ₀ = -1.7e-3 λ ^K ₁ = -3.8e-4 λ ^B = S	λ ^K ₀ = -1.1e-3 λ ^K ₁ = S λ ^B = S	λ ^K ₀ = -7.2e-4 λ ^K ₁ = S λ ^B = S	λ ^K ₀ = -6.1e-4 λ ^K ₁ = S λ ^B = U ₄₇₋₄₇	λ ^K ₀ = -6.8e-4 λ ^K ₁ = -2.7e-4 λ ^B = U ₄₆₋₄₈	
174	λ ^K ₀ = -5.5e-4 λ ^K ₁ = -5.1e-4 λ ^B = S	λ ^K ₀ = -4.9e-5 λ ^K ₁ = -4.5e-5 λ ^B = S	λ ^K ₀ = -3.7e-5 λ ^K ₁ = -2.4e-5 λ ^B = S	λ ^K _{0,1} = S λ ^B = S	λ ^K ₀ = -1.2e-4 λ ^K ₁ = -1.9e-4 λ ^B = U ₄₆₋₄₇	λ ^K ₀ = -1.0e-3 λ ^K ₁ = -1.5e-3 λ ^B = U ₄₅₋₄₈

Table 9-6: Fixed-boundary stability results in the I_p, - β plane. Orange blocks indicate unstable cases. The λ^K_{0,1} are kink unstable eigenvalues for the n=0 and n=1 families. λ^K_{0,1} = S => kink stability. λ^B = U_{i-j} => ballooning modes on surface numbers i – j (out of 49) are unstable. λ^B = S => ballooning stability. There are many unstable cases, and no stable path to I_p = 174 kA, β = 4.0%

9.4 Robustness of Performance as Plasma Profiles are Varied

For the results presented so far, the current and pressure profiles have had the same form as the reference li383 profiles. Now we investigate the effect on plasma performance of choosing plasma profiles that are different from the reference profiles. First, we examine the performance of plasmas supported by NCSX coils for a range of current profiles, with the pressure profile held fixed equal to the reference form shown in Figure 9-2. The effect of varying the current profile in the core region of the plasma is considered separately from the effect of varying the current profile in the edge region. In another set of experiments the effect of varying the pressure profile is considered, with the current profile held fixed equal to its reference form, also shown in Figure 9-2. We will show that good plasma performance is obtained for a wide range of current and pressure profiles. This allays any concern that the optimization methods used for designing the plasma configuration and coil system have produced only a narrow operating space of good performance plasmas.

9.4.1 Variation of the Current Profile in the Core Region

Here we examine the performance of plasmas supported by NCSX coils for current profiles which differ from the reference form mainly in the core region. A 1-parameter family of current profiles, J_α , is conveniently defined by

$$J_\alpha(s) = (1-\alpha) J^{\text{ref}}(s) + \alpha J^{\text{peaked}}(s),$$

where $0 \leq \alpha \leq 1$, and $J(s)$ denotes the surface averaged parallel current profile $\mathbf{J} \cdot \mathbf{B}$. As α ranges from zero to one, J_α undergoes a substantial change in shape, from the reference hollow current profile, J^{ref} , to a peaked current profile defined as $J^{\text{ref}} = 1 - s^2$. A plot of the J_α used in this study is shown in Figure 9-7.

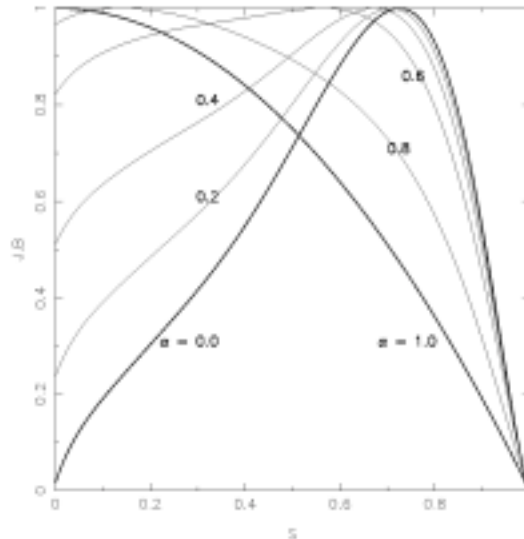


Figure 9-7: 1-parameter family of current profiles which vary mainly in the core region . The stable range of current profiles is $0 \leq \alpha \leq 0.5$. For this range of α , the internal inductance ℓ_i of an equivalent tokamak with the same average elongation, triangularity, and aspect ratio ranges from 0.30 to 0.54

With $\alpha = 0.0$, $J_\alpha = J^{\text{ref}}$ and the plasma configuration is identical to the reference configuration. As discussed in Section 9.3, the free-boundary β -limit for these profiles is at least $\beta = 5.0\%$. We execute a sequence of free-boundary optimizer runs, increasing α from 0.0 in steps of 0.2, to determine the range of values of α (i.e., range of current profiles) for which NCSX plasmas are stable at $\beta = 3.0\%$. For each run, the plasma current was held fixed at $I_p = 174$ kA, and the average toroidal field at $R = 1.4$ m is $B_T = 1.7$ T.

Table 9-7 shows a summary of the kink and ballooning stability properties for the various optimized configurations, including values of the effective ripple ϵ_h . It is seen that current profiles with $0 \leq \alpha \leq 0.5$ are stable to kink and ballooning modes, with quasi-axisymmetry measure $\epsilon_h < 1.3\%$ at $s=0.5$.

α	0.0	0.1	0.2	0.3	0.4	0.5	0.6	0.7
$\lambda_{0,1}^K$	S	S	S	S	S	S	-7.3e-4	-9.1e-4
$\lambda_{0,1}^B$	S	S	S	S	-1.5e-5	-2.8e-5	-5.1e-5	-8.0e-5
λ_B	S	S	S	S	S	S	S	S
$\epsilon_h[\%]$	0.44 1.29 2.97	0.37 1.16 3.11	0.22 0.90 2.39	0.21 0.88 2.24	0.33 1.32 3.84	0.36 1.27 3.63	0.38 1.13 3.11	0.34 1.05 2.71
TF [A]	-1.952e+5	-1.570e+5	-4.396e+4	-9.608e+4	-7.743e+4	-1.508e+5	-6.672e+4	-3.516e+4
Mod 1 [A]	-5.701e+5	-5.692e+5	-5.679e+5	-5.711e+5	-5.687e+5	-5.788e+5	-5.920e+5	-5.794e+5
Mod 2 [A]	-5.730e+5	-5.695e+5	-5.553e+5	-5.617e+5	-5.580e+5	-5.668e+5	-5.599e+5	-5.845e+5
Mod 3 [A]	-6.002e+5	-5.915e+5	-5.809e+5	-5.850e+5	-5.985e+5	-5.839e+5	-5.878e+5	-5.894e+5
Mod 4 [A]	-5.384e+5	-5.492e+5	-5.659e+5	-5.580e+5	-5.373e+5	-5.576e+5	-5.435e+5	-5.446e+5
PF Dipole	+2.434e-1	+3.467e-1	+2.152e-1	+2.254e-1	+2.878e-1	+3.218e-1	+2.606e-1	+2.423e-1
PF Quad	+1.097e-1	+6.088e-2	-7.816e-2	-1.420e-1	-2.717e-1	-4.003e-1	-3.071e-1	-4.889e-1
PF Hex	+1.515e+0	+2.813e+0	+1.995e+0	+2.910e+0	+2.050e+0	+3.275e+0	+3.185e+0	+4.122e+0
PF Oct	-9.098e+0	-8.298e+0	-1.682e+0	-2.132e+0	-4.230e+0	-4.626e+0	-3.256e+0	-1.588e+0

Table 9-7: Maximum growth rates for kink and ballooning modes ($\lambda_{0,1}^K, \lambda^B$), optimized values of effective ripple ($\epsilon_h[\%]$) at the $s=0.25$, $s=0.5$, and $s=0.75$ surfaces, and coil currents for various current profiles parameterized by the peakedness parameter α . All equilibria correspond to $\beta = 3.0\%$. Unstable cases are shown as yellow

For reasons of computational speed, the TERPSICHORE stability calculations in the optimizer which led to the eigenvalues tabulated in Table 9-7 used 49 radial grid points and 91 modes to represent the perturbation. To gain confidence that the reported range of stable current profiles really is truly defined by $0 \leq \alpha \leq 0.5$, we have re-optimized the configurations using

artificial multipliers for the kink and ballooning terms in δW (see Chapter 5) with $\text{COEC}=\text{COEP}=1.05$. The new configurations are minimally modified and have similarly small eigenvalues (actually smaller for the re-optimized $\alpha=0.5$ configuration). Further convergence tests will be made using more radial grid points and a greater number of perturbation modes but the main findings are expected to remain valid.

Figure 9-8 shows an overlay of plasma boundaries and calculated iota profiles for the $\alpha < 0.5$ stable configurations. The onset of instability may be correlated with a lack of adequate shear in the iota profile for $\alpha > 0.5$.

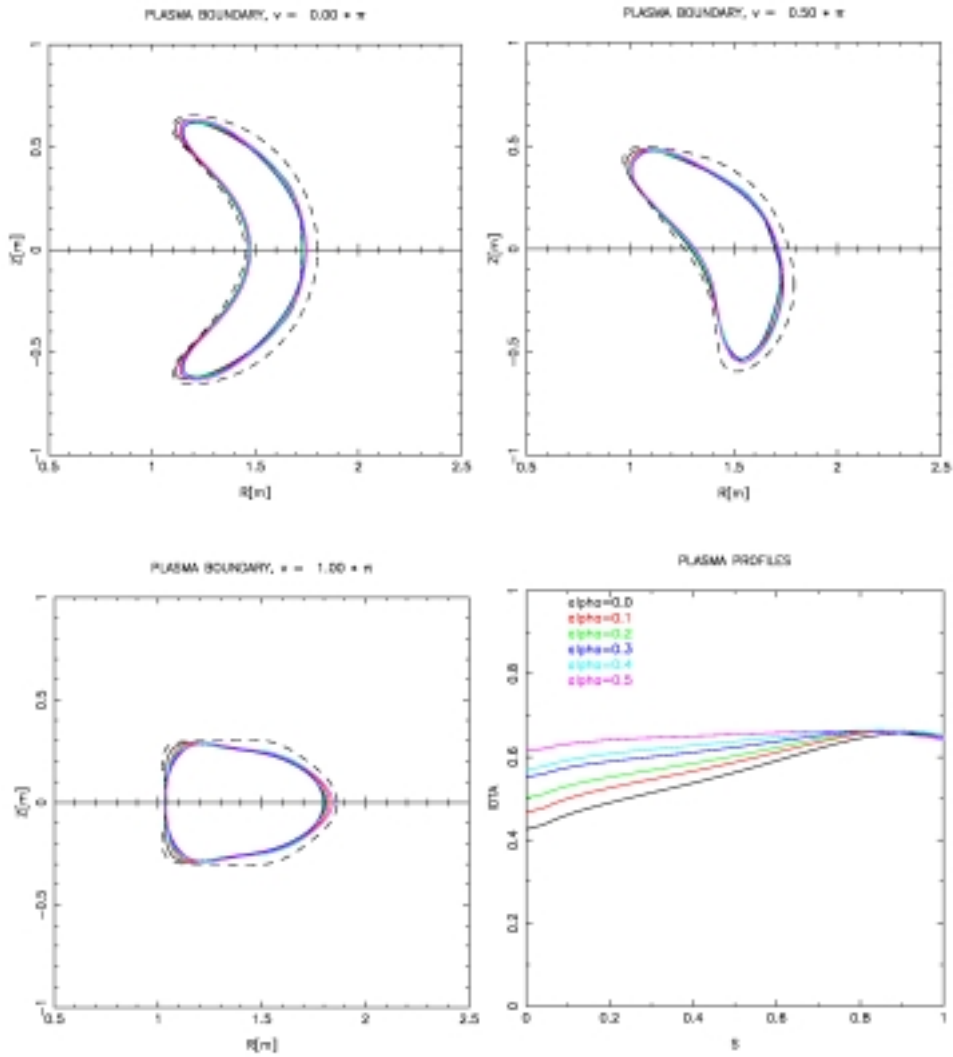


Figure 9-8: Overlay of plasma boundaries for stable equilibria at $\beta = 3.0\%$ for the J_α sequence of current profiles (where $\mathbf{J} \cdot \mathbf{B}$ is varied in the core region). The calculated iota profiles are also shown.

9.4.2 Variation of the Current Profile in the Edge Region

We now explore the effect of varying the current profile in the edge region. In particular we consider the family of current profiles, J_δ , shown in Figure 9-9 where

$$J_\delta(s) \propto J^{\text{ref}}(s) + \delta J^{\text{edge}}(s),$$

and $J^{\text{edge}}(s) = s^8$ gives a sizeable contribution to the current profile near the plasma edge. The values of δ shown in Figure 9-9 represent the magnitude of J_δ at the plasma edge relative to the maximum value of $J_\delta(s)$. δ varies from 0.0 to 0.5 in steps of 0.1.

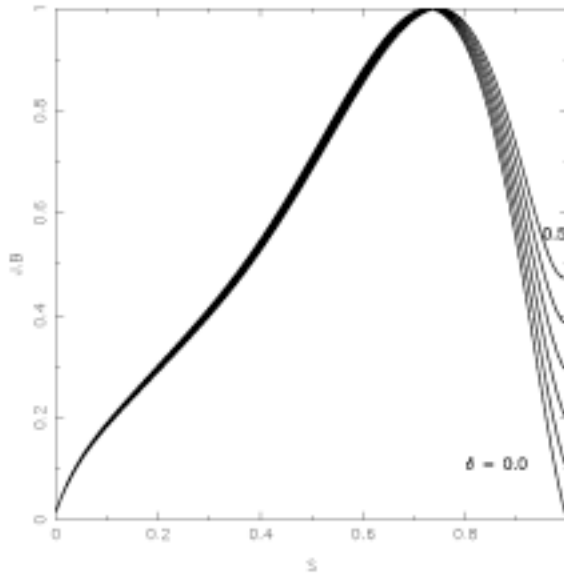


Figure 9-9: Family of current profiles $J_\delta(s)$ which vary mainly in the edge region. Stability may be enhanced as the edge current builds due to an increase in the global shear.

Whereas in Section 9.4.1 we considered free-boundary equilibrium reconstructions at $\beta = 3.0\%$, in this section we explore the stability characteristics of free-boundary plasmas with finite edge current at $\beta = 5.0\%$, a value which exceeds the reference fixed-boundary β -limit for li383.

Already the $I_p - \beta$ scan presented in Table 9-4 has shown a stable configuration with $I_p = 174$ kA, $\beta = 5.0\%$. Coil currents for this case are shown in Table 9-8. Using the same coil currents the free-boundary VMEC code was used to obtain free-boundary equilibria for each of the six current profiles shown in Figure 9-9. For each equilibrium $I_p = 174$ kA, $\beta = 5.0\%$, and the pressure profile was fixed equal to the reference form.

For each current profile the calculated equilibrium was stable to kink and ballooning modes.

AUX TF [A]	MOD 1 [A]	MOD 2 [A]	MOD 3 [A]	MOD 4 [A]	PF - DIPOLE	PF - QUAD	PF - HEX	PF - OCT
+2.053e+3	-5.658e+5	-5.767e+5	-5.555e+5	-5.498e+5	+1.212e-1	+4.957e-2	+3.075e-1	-5.400e-1

Table 9-8: Coil currents corresponding to the stable configuration with $I_p = 174\text{kA}$, $\beta = 5.0\%$ presented in Table 9-4. These currents are used in free-boundary equilibrium reconstructions which vary the edge current density.

The robust stability for the sequence of equilibria with different edge current densities can be understood in terms of the effect on the iota profile of adding successive current layers to the plasma edge region. Figure 9-10 shows overlays of the plasma boundaries and profiles of $\iota(s)$ for the six equilibria. In particular it should be noted that as more edge current is included, the shear $\iota'(s)$ in the edge region of the plasma is increased with no change to the edge iota. Such an increase in shear is known to be stabilizing for current-carrying stellarators (see ref. [2] and results presented in Chapter 5).

An increase in current density near the plasma edge is an expected consequence of a transition from L-Mode to H-Mode profiles. In view of the observations made above, there is an interesting possibility that such a transition will have beneficial effects on MHD stability. Future calculations should calculate β -limits for realistic models of H-mode profiles in NCSX.

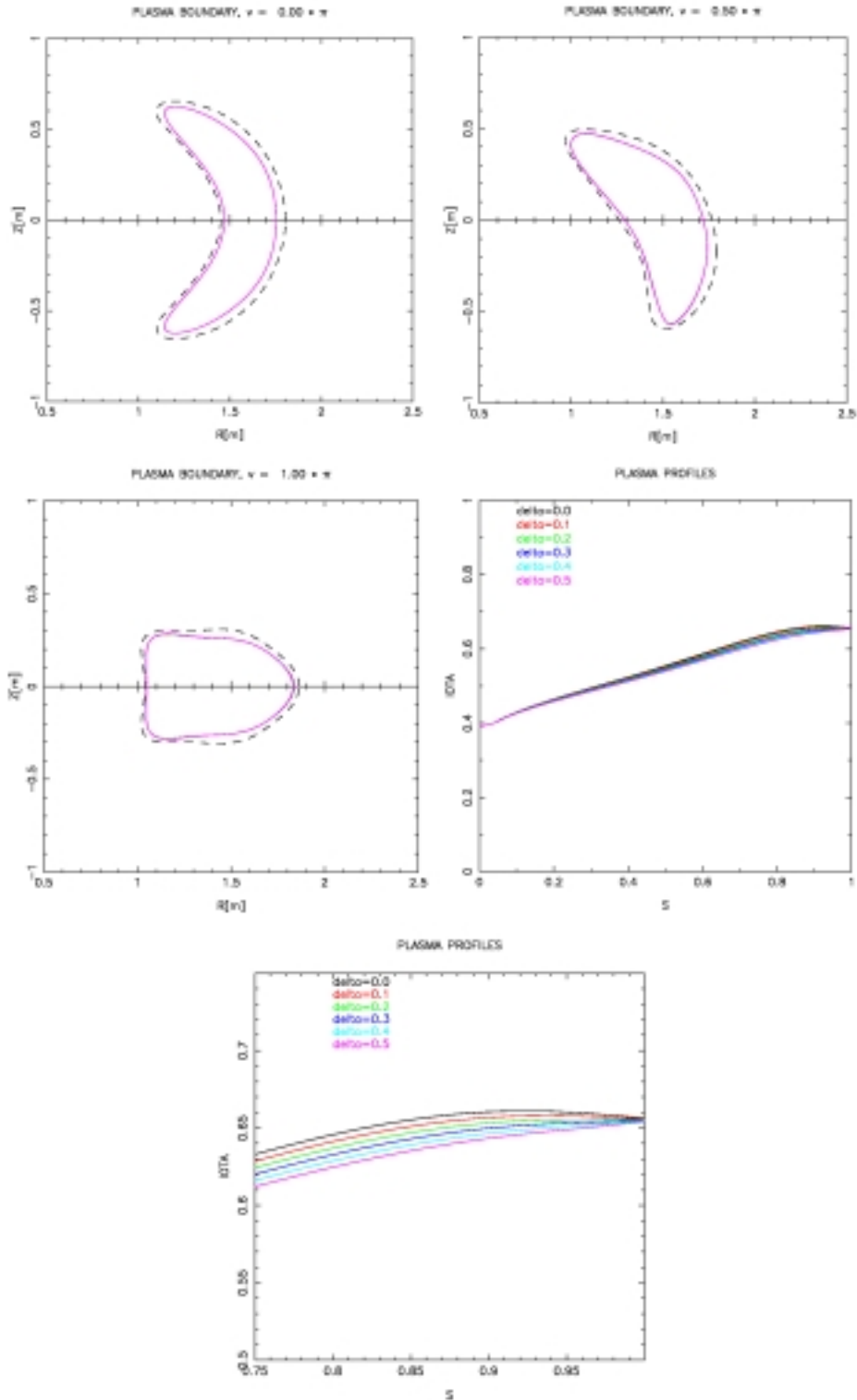


Figure 9-10: Overlay of plasma boundaries for six stable equilibria with varying edge current densities and $I_p = 174$ kA, $\beta = 5.0\%$. The coil currents are the same in all cases. The plasma boundaries vary little. Also shown are the $t(s)$ profiles (shown plotted in two frames, the second of which is a blow-up of the first). As the edge current is increased, the shear increases, which is a stabilizing effect

9.4.3 Variation of the Pressure Profile

As a third set of numerical experiments we examine the performance of plasmas supported by NCSX coils for a range of pressure profiles. The current profile shape is held fixed equal to the reference form. A 1-parameter family of pressure profiles is defined by

$$P_\gamma(s) = (1 - \gamma) P^{\text{ref}}(s) + \gamma P^{\text{peaked}}(s),$$

where $0 < \gamma < 1$, and P denotes the pressure profile $p(s)$. As γ ranges from zero to one, P_γ undergoes a change from the (broad) reference pressure profile to a more peaked pressure profile whose analytic dependence on toroidal flux is $P^{\text{peaked}} \propto (1 - s)^2$. This “peaked” form is a good fit with the NBI heated PBX-M discharge profile denoted by p_B in Section 9.2. A plot of the P_γ for different values of γ is shown in Figure 9-11.

We execute a sequence of free-boundary optimizer runs, increasing γ from 0.0 to 1.0 in steps of 0.2 to determine the range of values of γ (range of pressure profiles) for which NCSX plasmas supported by the designed coils are stable to ballooning and kink modes with optimized QA measure χ^2_{Bmn} at $\beta = 3.0\%$. As in subsection 9.4.1, we choose $I_p = 174$ kA, $\beta = 3.0\%$ with $B_T = 1.7$ T at $R = 1.4$ m, making no attempt to optimize β by changing I_p from this reference value.

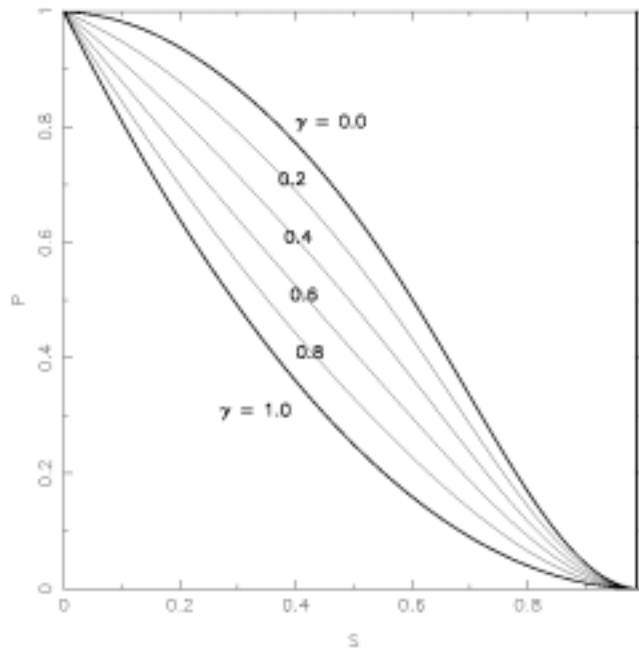


Figure 9-11: The 1-parameter family of pressure profiles, P_γ , for which plasma performance is evaluated at $\beta = 3\%$

Table 9-9 summarizes the optimizer runs as the peakedness parameter γ is varied. For the given parameterization of $p(s)$, stable configurations with good quasi-axisymmetry ($\epsilon_h < 1.1\%$ at $s=0.5$) were found for all cases except $\gamma=1.0$. For this case, we have found a stable configuration at $\beta = 2.5\%$. Figure 9-12 shows an overlay of the plasmas boundaries and iota profiles for each of the stable optimized configurations with $\gamma \leq 0.8$.

The operating space of stable configurations with $\beta = 3.0\%$, substantial variations in current and pressure profiles, and good quasi-symmetry appears to be quite broad. We also note that it should be possible to widen the operating space of stable profiles further by allowing the plasma current to vary in addition to the shape.

γ	0.0	0.2	0.4	0.6	0.8	1.0
λ^K_{0}	S	S	S	S	S	-3.0e-4
λ^K_{1}	S	S	S	S	S	-5.4e-5
λ_B	0	0	0	0*	0*	0*
ϵ_h [%]	0.33 0.80 1.83	0.22 0.72 1.78	0.23 0.78 1.91	0.31 1.05 2.56	0.25 0.73 1.60	0.25 0.62 1.29
TF [A]	-4.623e-1	-6.429e+1	-6.005e+1	-6.005e+1	+1.067e+3	-1.506e+4
Mod 1 [A]	-5.646e+5	-5.665e+5	-5.644e+5	-5.644e+5	-5.714e+5	-5.762e+5
Mod 2 [A]	-5.705e+5	-5.602e+5	-5.599e+5	-5.599e+5	-5.439e+5	-5.416e+5
Mod 3 [A]	-5.564e+5	-5.647e+5	-5.700e+5	-5.700e+5	-6.020e+5	-6.090e+5
Mod 4 [A]	-5.670e+5	-5.798e+5	-5.738e+5	-5.738e+5	-5.273e+5	-5.039e+5
PF Dipole	+1.250e-1	+1.235e-1	+1.326e-1	+1.326e-1	+1.043e-1	+4.353e-2
PF Quad	+2.787e-2	+2.660e-2	+7.660e-2	+7.660e-2	+2.587e-2	+3.271e-2
PF Hex	-2.737e-2	-4.365e-2	-1.759e-2	-1.759e-2	-9.751e-3	+4.737e-3
PF Oct	-1.017e-2	-9.667e-3	-9.695e-3	-9.695e-3	-4.849e-3	-1.207e-2

Table 9-9: Maximum growth rates for kink and ballooning modes ($\lambda^K_{0,1}$, λ^B), optimized values of effective ripple (ϵ_h [%]) at the $s=0.25$, $s=0.5$, and $s=0.75$ surfaces and coil currents for various pressure profiles parameterized by the peakedness parameter γ . $\lambda^B = 0^*$ denotes instability on first evaluated surface (out of 49) near the magnetic axis. All equilibria correspond to $\beta = 3.0\%$. Unstable cases are shown as yellow

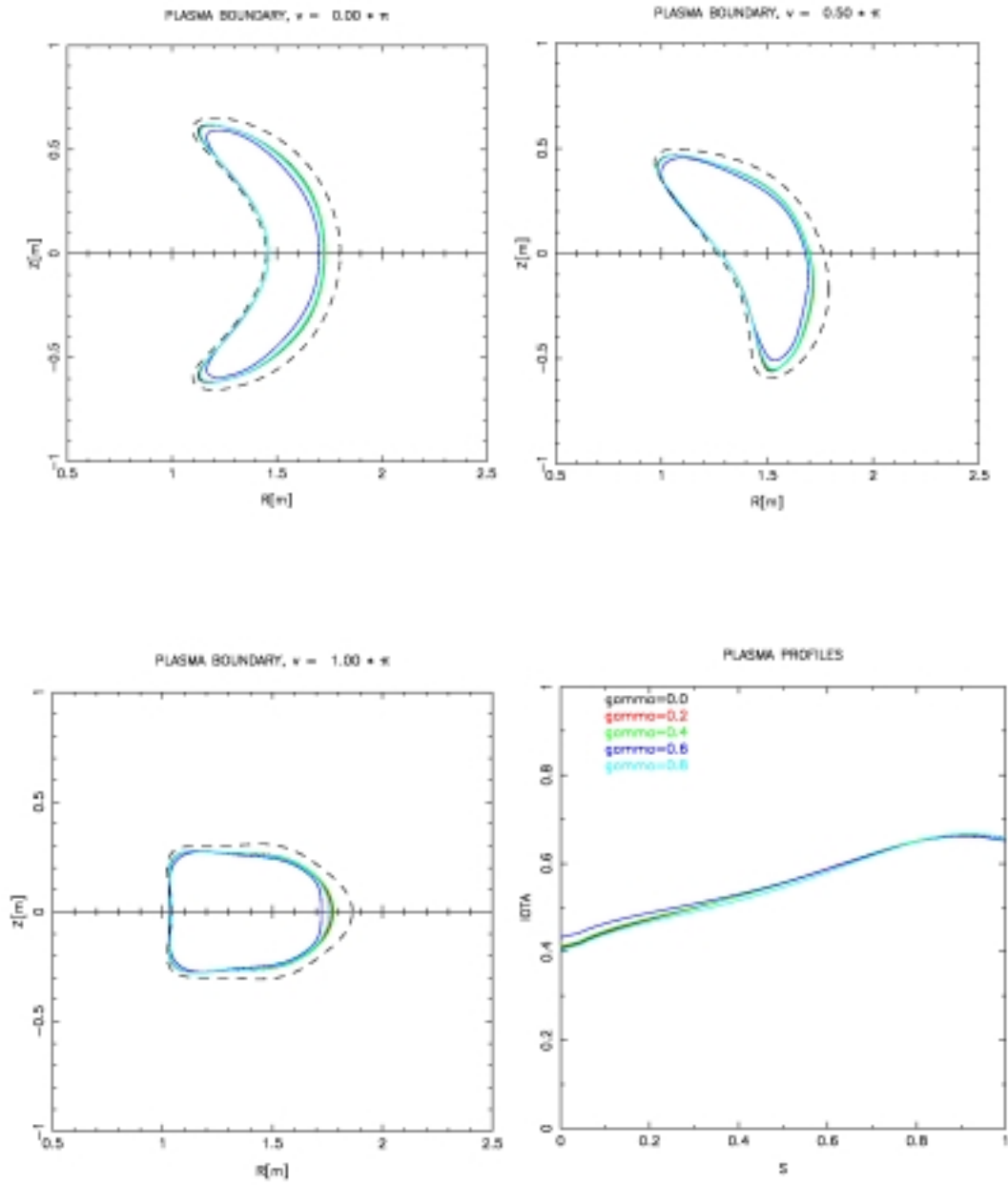


Figure 9-12: Overlay of plasma boundaries and iota profiles for stable optimized configurations of the pressure profile scan. $I_p = 174$ kA, $\beta = 3.0\%$ for all cases

9.5 Flexibility to Control the External Transform

We now demonstrate the important capability of NCSX coils to effect substantial changes in the external field contribution to $\iota(s)$. The MHD stability of stellarator plasmas can depend critically on details of the iota profile; for example on the location of the $\iota = 0.5$ magnetic surface. The W7AS experiments reported at IAEA2000 in Sorrento[3] demonstrate cases where stability depends, not on the magnitude of the external transform ι_{ext} , but on the ability to avoid $\iota(1) = 0.5$ during the discharge due to $q=2$ global tearing modes. On the other hand, the reference S3 configuration (full current, full beta) for NCSX has $\iota(0) = 0.44$, $\iota(1) = 0.65$, while the reference S1 “vacuum” configuration (see Chapter 10.2) has $\iota(s) < 0.5$ for all s values. Plasma evolution from S1 to S3 implies, for the reference scenario, passage through $\iota(1) = 0.5$. The NCSX coil currents can be chosen to evolve in such a way that 3D shaping of the plasma avoids the trigger of any kink mode. Nevertheless it is important to have the ability to control the iota profile through external shaping so that $\iota(1) = 0.5$ can be avoided, if that is found to be necessary. In Chapter 10.4 a “high iota” startup scenario is presented, which avoids passage through $\iota(1) = 0.5$. The ability to control $\iota(s)$ will be a very useful control knob to aid the mapping of stable/unstable boundaries for NCSX.

9.5.1 Variation of $\iota(s)$ at Fixed Shear

Here we demonstrate the ability to raise and lower $\iota(s)$ while keeping the shear essentially constant. As a baseline plasma we choose an S2 state with $I_p = 174$ kA, $\beta = 0.0\%$ that was generated from the reference li383 S3 configuration by ramping β from 4.2% to 0.0% while maintaining stability to kink and ballooning modes. The S2 state has axis and edge values of iota of $\iota(0) = 0.44$, $\iota(1) = 0.65$. As final preparation for the study a further optimization run was made where $\iota(0)$ and $\iota(1)$ were constrained to remain constant, the kink and ballooning constraints were turned off, and the configuration was re-optimized for χ^2_{Bmn} .

For the iota scan experiments we target desired values of $\iota(0)$ and $\iota(1)$, and optimize χ^2_{Bmn} , making no attempt to stabilize the kink and ballooning modes. The goal here is to explore coil flexibility, not plasma performance. The plasma current is held fixed at $I_p = 174$ kA, and the toroidally averaged B_T is held constant at 1.7 T at $R = 1.4$ m. (Increasing/decreasing $\iota(s)$ by changing B_T is trivial. However, changing $\iota(s)$ at fixed plasma current and toroidal field by changing the external transform using 3D shaping is not; this is the goal of the present flexibility studies). Figure 9-13 shows plasma boundaries and calculated iota profiles for cases where $\iota(s)$ was programmed to change both the axis and edge values of iota by ± 0.1 and ± 0.2 from the baseline S2 values. It is interesting to note the range of shapes required to produce the target iota profiles.

Table 9-10 presents a summary of the calculated coil currents and details of the calculated iota profiles. Presently NCSX plans for the auxiliary TF coils to provide ± 0.3 T, corresponding to $\text{TF}[A] = 2.1\text{e}+6$.

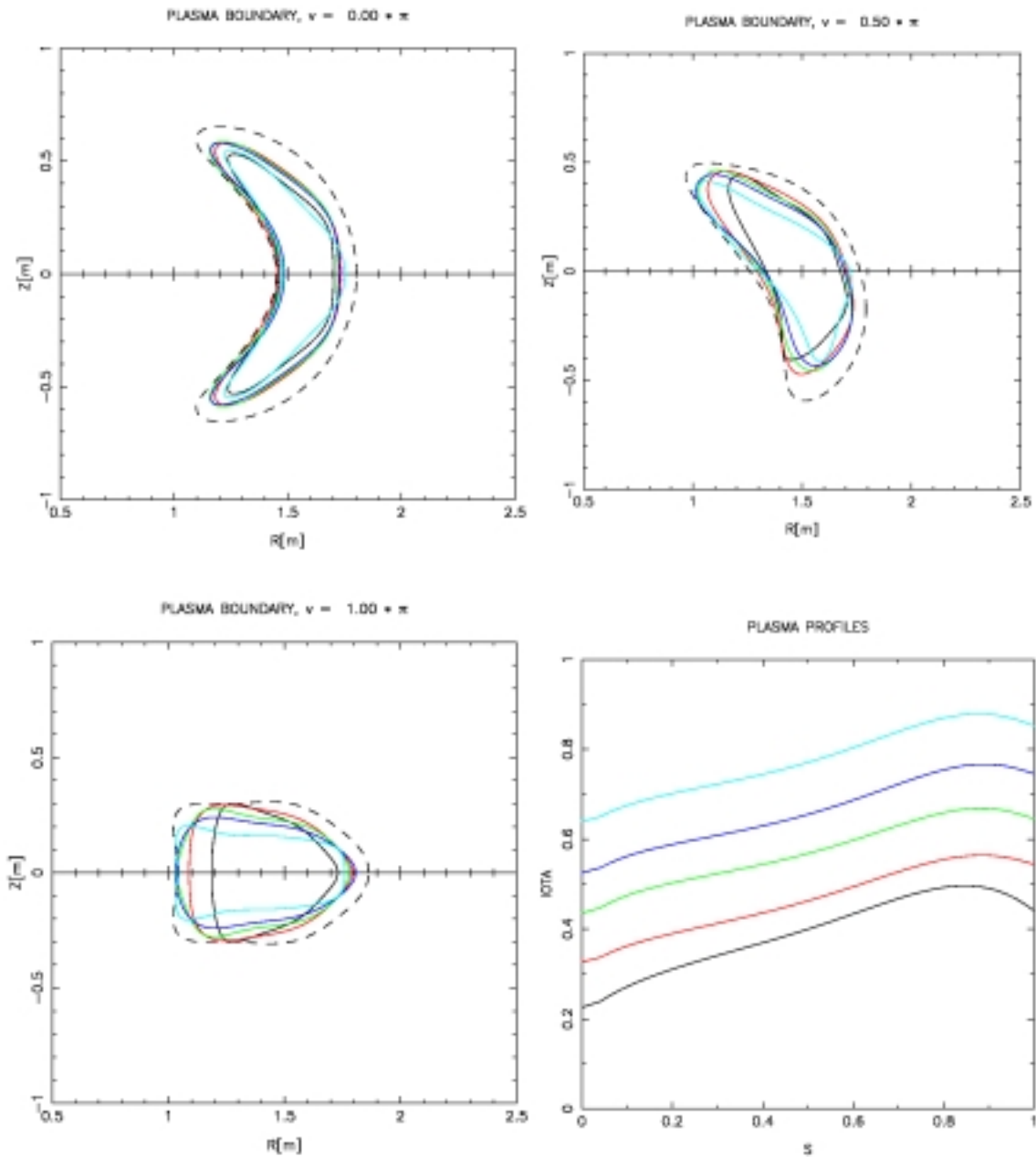


Figure 9-13: Plasma boundaries and iota profiles for iota-scan flexibility studies where coil currents are asked to change in such a way as to induce specified changes in $\iota(s)$. Here $\iota(s)$ is raised/lowered in such a way that the shear is preserved

	RUN 1	RUN 2	RUN 3	RUN 4	RUN 5
$\iota(0)$	0.23	0.33	0.44	0.53	0.64
$\iota(1)$	0.44	0.54	0.65	0.75	0.85
$\iota_{vac}(0)$	0.28	0.37	0.50	0.60	0.71
$\iota_{vac}(1)$	0.20	0.34	0.45	0.54	0.63
A	5.36	4.52	4.57	4.77	5.31
TF [A]	+2.944e+6	+1.462e+6	- 4.881e+2	- 7.960e+5	- 6.881e+5
Mod 1 [A]	- 4.156e+5	- 4.909e+5	- 5.690e+5	- 6.126e+5	- 6.217e+5
Mod 2 [A]	- 4.332e+5	- 4.954e+5	- 5.606e+5	- 5.958e+5	- 5.964e+5
Mod 3 [A]	- 4.375e+5	- 5.078e+5	- 5.906e+5	- 6.431e+5	- 5.971e+5
Mod 4 [A]	- 4.127e+5	- 4.842e+5	- 5.302e+5	- 5.428e+5	- 5.816e+5
PF Dipole	+ 7.061e-1	+ 5.370e-1	+ 4.251e-1	+ 3.880e-1	+ 1.512e-1
PF Quad	- 1.642e+0	- 2.237e-1	+ 3.553e-1	+1.000e+0	+3.019e+0
PF Hex	+1.023e+1	+4.348e+0	+3.003e+0	+3.336e+0	+2.819e+0
PF Oct	- 2.201e+1	- 8.434e+0	- 1.549e+1	- 1.695e+1	+2.068e+0

Table 9-10:Coil currents for raising/lowering $\iota(s)$ at constant shear (see Figure 9-13)

9.5.2 Variation of $\iota(s)$ at Fixed $\iota(0)$ – Changing the Shear

Figure 9-14 and Table 9-11 show results from a similar calculation, where now the axis value $\iota(0)$ is constrained to remain fixed at the nominal value $\iota(0) = 0.44$, and the edge value is increased/decreased from the nominal value of $\iota(1) = 0.65$ by ± 0.1 and ± 0.2 . The effect is to change the global shear.

	RUN 6	RUN 7	RUN 8	RUN 9	RUN 10
$\iota(0)$	0.43	0.44	0.44	0.44	0.44
$\iota(1)$	0.44	0.54	0.65	0.74	0.84
$\iota_{vac}(0)$	0.27	0.51	0.50	0.51	0.53
$\iota_{vac}(1)$	0.16	0.34	0.45	0.53	0.63
A	5.23	4.87	4.57	4.72	4.88
TF [A]	- 1.257e+2	+1.630e+4	- 4.881e+2	- 1.839e+4	- 6.188e+5
Mod 1 [A]	- 5.675e+5	- 5.694e+5	- 5.690e+5	- 5.632e+5	- 5.861e+5
Mod 2 [A]	- 5.734e+5	- 5.635e+5	- 5.606e+5	- 5.554e+5	- 5.769e+5
Mod 3 [A]	- 5.757e+5	- 6.019e+5	- 5.906e+5	- 5.764e+5	- 6.016e+5
Mod 4 [A]	- 5.850e+5	- 5.230e+5	- 5.302e+5	- 5.540e+5	- 5.995e+5
PF Dipole	+ 9.995e-1	+ 6.677e-1	+ 4.251e-1	+ 4.399e-1	+ 7.193e-1
PF Quad	- 1.717e+0	- 4.195e-1	+ 3.553e-1	+ 4.468e-1	- 3.596e-1
PF Hex	+1.605e+1	+9.640e+0	+3.003e+0	- 8.239e-2	+1.519e+0
PF Oct	- 2.123e+1	- 2.161e+1	- 1.549e+1	-4.620e+0	- 3.330e-1

Table 9-11: Coil currents for increasing/decreasing shear (see Figure 9-14)

The results in this section demonstrate a substantial capability for the M1017 coil set to scale the iota profile or change the shear. We have found similar flexibility to change the $\iota(s)$ profile for S1 states with $I_p = 0$ kA, a flexibility that is used to control $\iota(s)$ in the high-iota startup scenario presented in Chapter 10.

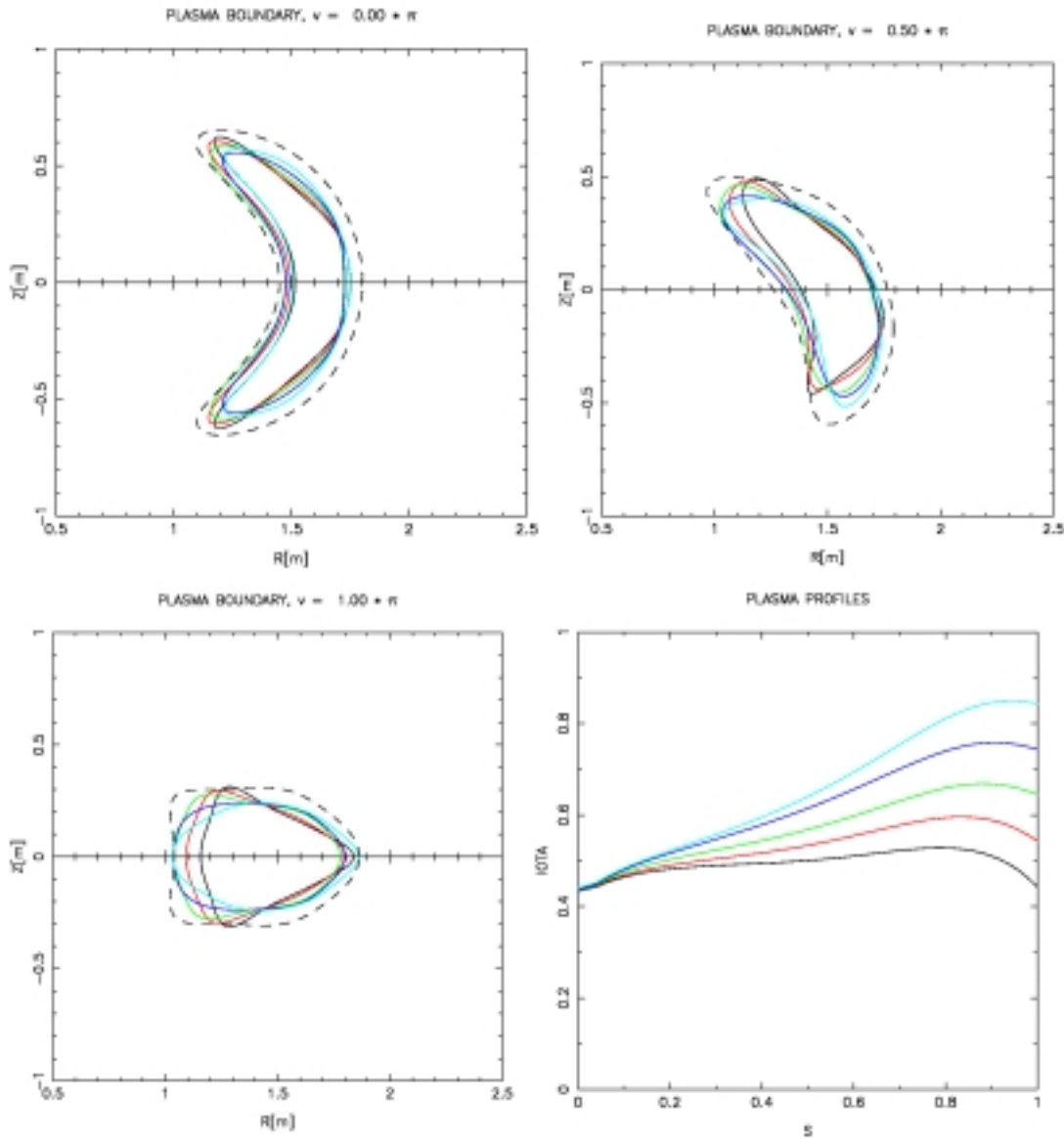


Figure 9-14: Plasma boundaries and iota profiles for iota-scan flexibility studies where coil currents are asked to change in such a way as to induce specified changes in $\iota(s)$. Here the shear is increased/decreased

9.6 Flexibility to Study Kink Stabilization by 3D Shaping

The free-boundary $I_p - \beta$ scan numerical experiments presented in the Section 9.3 and summarized in Table 9-4 can be used to clearly demonstrate the effect of MHD stabilization by 3D shaping and to suggest controlled experiments to explore stability boundaries in NCSX.

The present measure used for stability in the free-boundary optimizer cost function is a weighted sum of the square of the maximum unstable kink mode eigenvalue and the sum (over ballooning unstable surfaces) of the maximum ballooning mode eigenvalue. It follows that any stable “final state” of the optimizer is a state of marginal stability. Consider two states from the $I_p - \beta$ scan that have the same value of plasma current but different values of beta. For example the cases $I_p = 43.5$ kA, $\beta = 1.0\%$, and $I_p = 43.5$ kA, $\beta = 3.0\%$. The plasma shapes differ (see Fig. 9-15). Each plasma is at the β -limit for its given shape.

Figure 9-15 also shows the calculated $\iota(s)$ profiles. Axis and edge iota values are:

$$\begin{aligned}\iota(0) &= 0.44, \iota(1) = 0.50 \text{ for } I_p = 43.5 \text{ kA, } \beta = 1.0\%; \\ \iota(0) &= 0.40, \iota(1) = 0.44 \text{ for } I_p = 43.5 \text{ kA, } \beta = 3.0\%.\end{aligned}$$

The calculated coil currents for these two configurations are presented in the first two columns of Table 9-12.

Now consider the effect of taking the $I_p = 43.5$ kA, $\beta = 1.0\%$ configuration and raising β to 3.0% while keeping the plasma boundary fixed. The iota profile for this $\beta = 3.0\%$ “virtual” configuration is found to have $\iota(0) = 0.40$, $\iota(1) = 0.50$. It is strongly unstable to kink modes, with maximum eigenvalues for the $n=0$ and $n=1$ families of $\lambda^K_0 = -5.68e-4$, and $\lambda^K_1 = -1.28e-3$. Ballooning modes are also found over the range of magnetic surfaces from $s = 0.14$ to $s = 0.33$, and the ripple strength at $s=0.25$, $s=0.5$ and $s=0.75$ increases to $\epsilon_h = 2.10\%$, 5.28% and 12.9% (compared with $\epsilon_h = 0.44\%$, 1.30% and 2.90% - see Table 9-4). Comparing the iota profile of the fixed boundary $\beta = 3.0\%$ virtual configuration with the iota profiles of the free boundary $\beta = 1.0\%$ and free-boundary $\beta = 3.0\%$ configurations shows that raising beta at fixed shape has predominantly changed the transform on axis whereas the edge transform has remained unchanged. It follows that the change in shape and the change in external transform induced by the change in coil current between the $I_p = 43.5$ kA, $\beta = 1.0\%$ free-boundary configuration and the $I_p = 43.5$ kA, $\beta = 3.0\%$ free-boundary configuration are responsible for the stabilization of the higher β configuration.

We have remarked that the $\iota(s)$ profile for the $I_p = 43.5$ kA, $\beta = 1.0\%$ free-boundary configuration has $\iota(1) = 0.50$. The question naturally arises whether the reduced β -limit of this configuration compared with the $I_p = 43.5$ kA, $\beta = 1.0\%$ free-boundary configuration, which had $\iota(1) = 0.44$, is due to the destabilizing influence of the $\iota(1) = 1/2$ rational surface. The flexibility of the NCSX modular coil set to change the iota profile (demonstrated in Section 9.5) can be used to test such a question. The free-boundary optimizer was re-run for the case $I_p = 43.5$ kA, $\beta = 1.0\%$, with the additional constraint that the plasma shape consistent with the coil currents be such that $\iota(1) = 0.44$. A successful solution was found with $\iota(0) = 0.45$, $\iota(1) = 0.45$ and $\iota_{\max} =$

0.46 at $s = 0.65$. The coil currents for this modified configuration are shown in the third column of Table 9-12. The constrained configuration was verified to be marginally stable by freezing the plasma boundary, increasing β , and verifying the emergence of a kink instability. If the β is increased to 3.0% in this modified configuration, we find $\iota(0) = 0.41$, $\iota(1) = 0.45$ and $\iota_{\max} = 0.47$ at $s = 0.58$. Thus the $\Delta\iota$ due to shaping, as opposed to profile changes, is essentially zero on axis and zero at the edge. Overlays of the constrained $I_p = 43.5$ kA, $\beta = 1.0\%$ low β -limit configuration and the marginally stable $I_p = 43.5$ kA, $\beta = 3.0\%$ configuration, as well as the calculated $\iota(s)$ profiles are shown in Figure 9-16. Stabilization at the enhanced β is due to 3D shaping.

The ability to investigate the stabilizing role of 3D shaping is an important element of the experimental program of NCSX. Investigations of this type allow testing and investigation of the stability boundaries of NCSX at low β .

	$I_p = 43.5$ KA $\beta = 1.0\%$	$I_p = 43.5$ KA $\beta = 3.0\%$	$I_p = 43.5$ KA $\beta = 1.0\%$ $\iota(1)$ constrained
$\iota(0)$	0.44	0.40	0.45
$\iota(1)$	0.50	0.44	0.45
Aux TF [A]	- 3.117e+2	+6.004e+3	+6.645e+3
Mod 1 [A]	- 5.657e+5	- 5.598e+5	- 5.742e+5
Mod 2 [A]	- 5.764e+5	- 5.773e+5	- 5.638e+5
Mod 3 [A]	- 5.268e+5	- 5.717e+5	- 5.921e+5
Mod 4 [A]	- 6.350e+5	- 5.460e+5	- 5.457e+5
PF Dipole	+ 5.868e-1	+ 3.051e-1	+ 5.778e-1
PF Quad	+ 9.193e-1	- 1.234e-1	+ 9.587e-1
PF Hex	- 6.159e-1	+ 7.277e-1	+ 1.536e-1
PF Oct	+1.416e+0	+1.564e+0	- 9.332e+0

Table 9-12: Coil currents for cases illustrating MHD stabilization by 3D shaping. Units for the Auxiliary TF and Modular coil currents are amps. Poloidal field “currents” are expressed as multipole moments

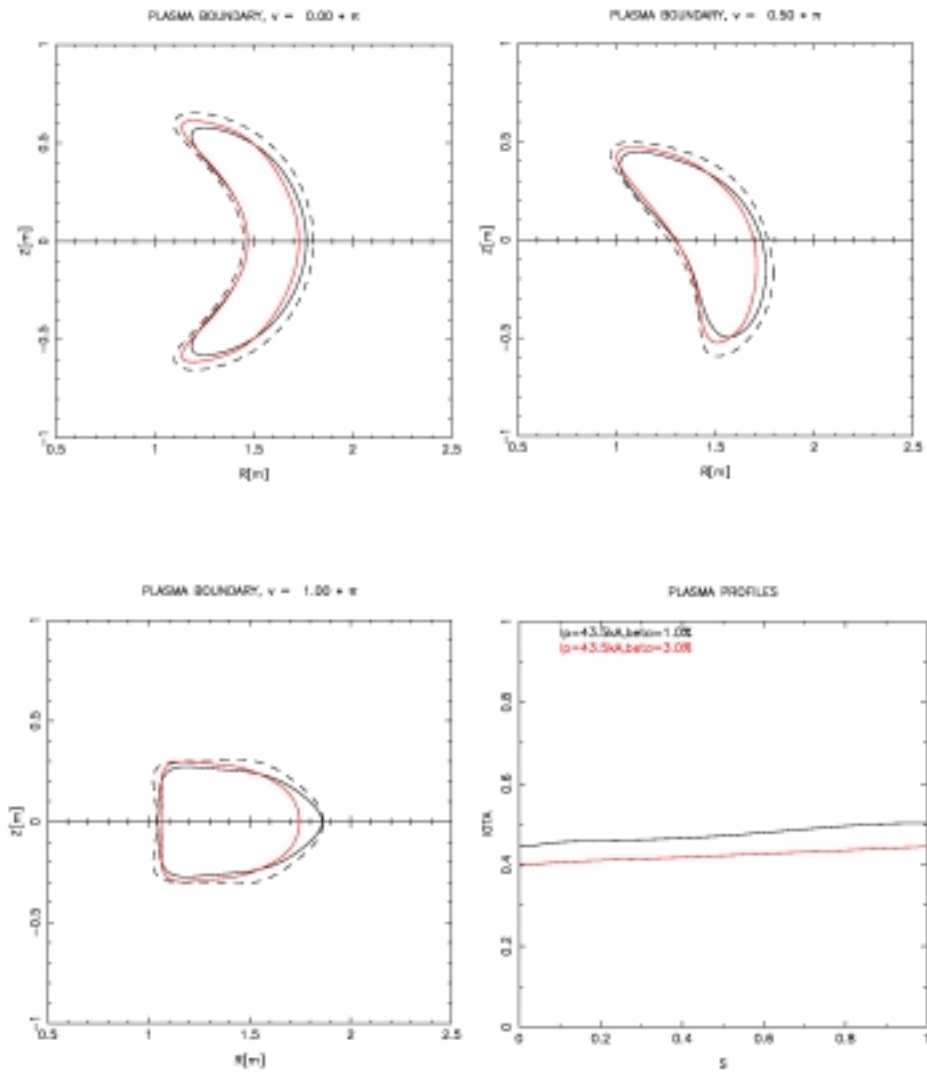


Figure 9-15: Overlay of plasma boundaries and iota profiles for the cases $I_p = 43.5$ kA, $\beta = 1.0\%$ and $I_p = 43.5$ kA, $\beta = 3.0\%$ used to illustrate MHD stabilization by 3D shaping

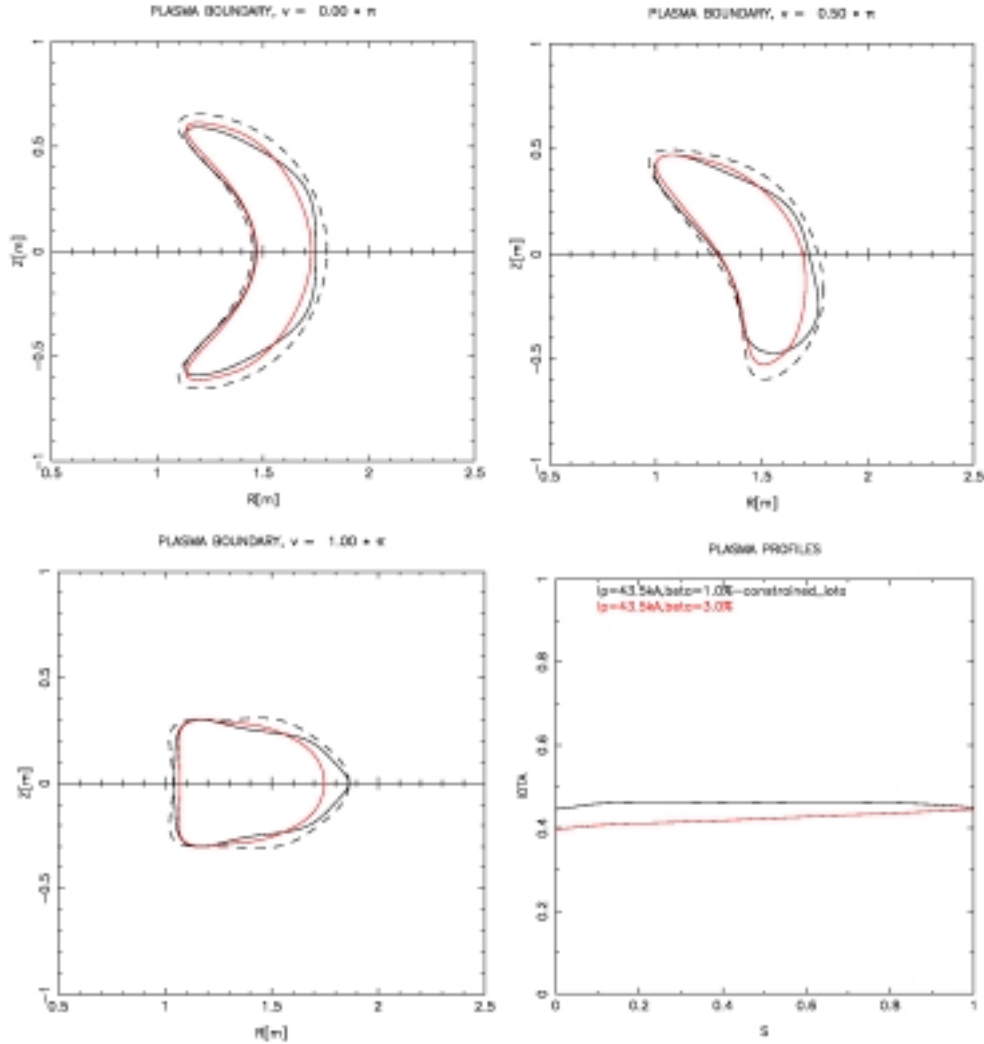


Figure 9-16: Overlay of plasma boundaries and iota profiles for the $\iota(1)=0.44$ constrained $I_p = 43.5$ kA, $\beta = 1.0\%$ configuration and the $I_p = 43.5$ kA, $\beta = 3.0\%$ configuration. These cases are used to show that the reason the unconstrained $I_p = 43.5$ kA, $\beta = 1.0\%$ configuration has a low β -limit relative to the $I_p = 43.5$ kA, $\beta = 3.0\%$ configuration (see Figure 9-15) is not due to the proximity of $\iota(1)$ to 0.5, but rather the change in 3D shape

9.7 Flexibility to Vary the Degree of Quasi-Axisymmetry

The ability to generate configurations with good quasi-axisymmetry is an essential requirement of the NCSX design. For a systematic exploration of the role of QA in improving the transport properties of stellarator plasmas, it is necessary to have the ability to control the degree of QA-ness. In this section we demonstrate this ability, by varying NCSX modular coil currents to induce plasma shape changes that degrade/enhance the QA-ness (measured by the

magnitude of the ripple amplitude, ϵ_h) while maintaining plasma stability to kink and ballooning modes.

Figure 9-17 shows an overlay of plasma boundaries for three configurations, each with $I_p = 43.5$ kA, $\beta = 3.0\%$, each with the same profiles of plasma current and pressure, but each exhibiting different degrees of quasi-axisymmetry. The ripple amplitude ϵ_h varies by a factor of 9 at the $s=0.25$ surface (normalized radius $r/a \approx 0.5$), and by a factor of about 4 at the $s=0.5$ surface. Values of ϵ_h and of the coil currents which support the equilibria are presented in Table 9-13. Each configuration is stable to kink and ballooning modes and was obtained using the free-boundary optimizer.

	CASE 1	CASE 2	CASE 3
ϵ_h [%]	0.44	2.50	3.99
	1.30	3.27	5.44
	2.90	5.15	8.33
Aux TF [A]	- 6.563e+2	+8.441e+3	- 4.191e+3
Mod 1 [A]	- 5.655e+5	- 5.227e+5	- 5.255e+5
Mod 2 [A]	- 5.742e+5	- 6.537e+5	- 6.562e+5
Mod 3 [A]	- 5.269e+5	- 5.510e+5	- 6.433e+5
Mod 4 [A]	- 6.351e+5	- 5.077e+5	- 2.812e+5
PF Dipole	+ 5.863e-1	+ 3.422e-1	+ 4.123e-1
PF Quad	+ 9.192e-1	- 9.626e-2	+ 3.618e-2
PF Hex	- 6.702e-1	+1.554e+0	+1.270e+0
PF Oct	+1.511e+0	+ 8.322e-2	+ 4.653e-1

Table 9-13: Three configurations with the same profiles of plasma current and pressure, each with $I_p = 43.5$ kA, $\beta = 3.0\%$, each stable to kink and ballooning modes, but each with different degrees of quasi-axisymmetry measured by the effective ripple ϵ_h measured at the $s=0.25$, $s=0.5$ and $s=0.75$ magnetic surfaces. CASE 1 is the optimized $I_p = 43.5$ kA, $\beta = 3.0\%$ case that appears in Table 9-4

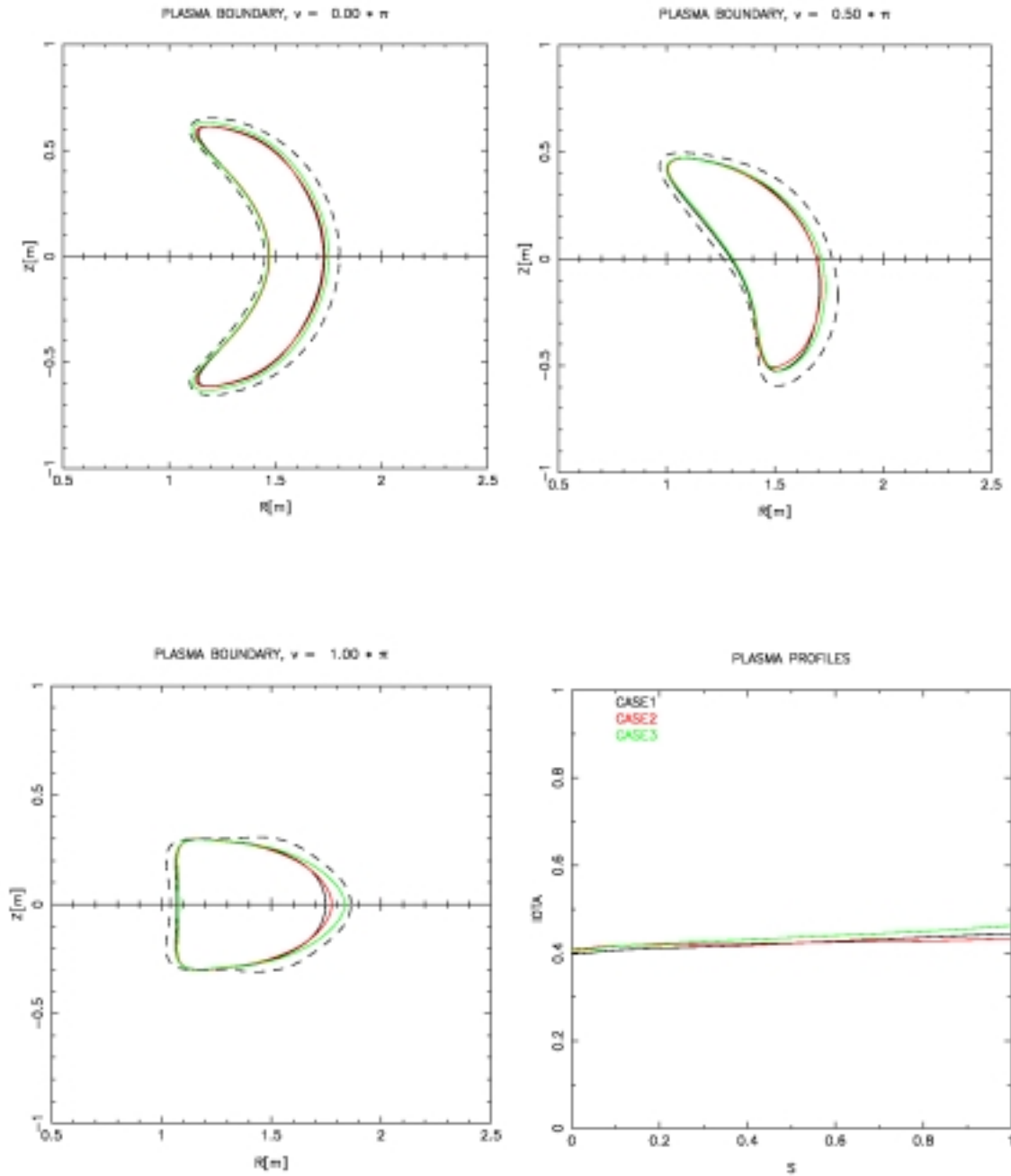


Figure 9-17: Overlay of plasma boundaries for three configurations with $I_p = 43.5$ kA, $\beta = 3.0\%$, the same profiles of plasma current and pressure, but different levels of quasi-axisymmetry (see Table 9-13). Each configuration is stable to kink and ballooning modes

9.8 Summary

We have presented a number of numerical experiments that demonstrate the ability of NCSX coils to meet the NCSX project mission. We have shown

- The NCSX plasma shape/position is robust with respect to uncertainties in the match between plasma profiles and assumed coil currents – e.g., the plasma boundaries displayed in Figure 9-4 were obtained using a variety of assumed plasma profiles and show modest changes in shape/position, whereas Tables 9-7 and 9-9 show the variation in coil currents required for optimized plasmas with different profiles when plasmas are further constrained to be limited by the first wall boundary.
- Using reference S3 plasma profiles there is a wide operating space of I_p , β values for which plasmas supported by NCSX coils are stable to kink and ballooning modes with low helical ripple amplitude ϵ_h (see Table 9-4).
- NCSX plasma performance is robust with respect to substantial variations in plasma current and pressure profile shape (see Tables 9-7 and 9-9) and the discussion of finite edge current in Section 9.4.2.
- Substantial changes in the external transform $\iota(s)$ and shear $\iota'(s)$ can be induced (see Tables 9-10 and 9-11, and corresponding figures) by varying currents in the NCSX coils. This provides a significant control knob for the experimental determination of stable/unstable operating boundaries and the investigation of 3D shape stabilization.
- NCSX coils have good flexibility to stability boundaries, and to explore the role of 3D shaping in stabilizing MHD modes, see Section 9.6.
- NCSX coils have the flexibility to control the degree of quasi-axisymmetry allowing exploration of the physics of QA plasmas, see Section 9.7.

References

- [1] D. Mikkelsen “Standard Profiles for NCSX Flexibility Studies”, March 1 2000
<http://www.pppl.gov/ncsx/ncsxfss/Physics/physics.html>
- [2] M.I. Mikhailov, V.D. Shafranov “Stable Current Profile in a Stellarator with Shear”, Nucl. Fusion 30, 413 421 (1990).
- [3] R. Jaenicke et al., “Operational Boundaries on the Stellarator W7-AS at the Beginning of the Divertor Experiments”, 18th IAEA Fusion Energy Conference, Sorrento, Italy, 4-10 Oct 2000, Paper IAEA-CN-77/OV4/3.